 Click here to access/download;Title Page;Title Page.docx

Development of lipidoid nanoparticles for siRNA delivery to neural cells

Purva Khare,[1] Kandarp M. Dave,[1] Yashika S. Kamte,[1] Muthiah A. Manoharan,[2] Lauren A. O'Donnell,[1] Devika S Manickam[1†]

[1]Graduate School of Pharmaceutical Sciences, Duquesne University, Pittsburgh, PA, USA.

[2]Alnylam Pharmaceuticals, Cambridge, MA, USA.

†**Corresponding author**: Devika S Manickam
453 Mellon Hall, 600 Forbes Avenue,
Pittsburgh, PA 15282.
Email: soundaramanickd@duq.edu
Twitter @manickam_lab
Phone: +1 (412) 396-4722, Fax +1 (412) 396-2501

Manuscript Body
Click here to access/download;Manuscript Body;Revision_Manuscript Body.pdf

Abstract

Lipidoid nanoparticles (LNPs) are the delivery platform in Onpattro, the first FDA-approved siRNA drug. LNPs are also the carriers in the Pfizer-BioNTech and Moderna COVID-19 mRNA vaccines. While these applications have demonstrated that LNPs effectively deliver nucleic acids to hepatic and muscle cells, it is unclear if LNPs could be used for delivery of siRNA to neural cells, which are notoriously challenging delivery targets. Therefore, the purpose of this study was to determine if LNPs could efficiently deliver siRNA to neurons. Because of their potential utility in either applications in the central nervous system and the peripheral nervous system, we used both cortical neurons and sensory neurons. We prepared siRNA-LNPs using C12-200, a benchmark ionizable cationic lipidoid along with helper lipids. We demonstrated using dynamic light scattering that the inclusion of both siRNA and PEG-lipid provided a stabilizing effect to the LNP particle diameters and polydispersity indices by minimizing aggregation. We found that siRNA-LNPs were safely tolerated by primary dorsal root ganglion neurons. Flow cytometry analysis revealed that Cy5 siRNA delivered via LNPs into rat primary cortical neurons showed uptake levels similar to Lipofectamine RNAiMAX—the gold standard commercial transfection agent. However, LNPs demonstrated a superior safety profile whereas the Lipofectamine-mediated uptake was concomitant with significant toxicity. Fluorescence microscopy demonstrated a time-dependent increase in the uptake of LNP-delivered Cy5 siRNA in a human cortical neuron cell line. Overall, our results suggest that LNPs are a viable platform that can be optimized for delivery of therapeutic siRNAs to neural cells.

Keywords

Lipidoid nanoparticle, C12-200, siRNA, neural cell, transfection

24 **Introduction**

25

26 Delivery of small interfering RNA (siRNA) is a promising strategy to treat pathologies as it
27 allows genetic manipulation with a greater degree of target specificity with fewer off-target effects
28 (1, 2). Lipidoid nanoparticles (LNPs) are the carriers in Onpattro, the first LNP-based RNAi drug
29 to gain FDA approval for the treatment of polyneuropathies caused by a rare and life-threatening
30 disorder, hereditary transthyretin-mediated amyloidosis (3). The clinical utility of LNPs is further
31 reiterated by the recent full and emergency FDA approvals of the Pfizer-BioNTech (Comirnaty)
32 and Moderna COVID-19 mRNA vaccines, respectively (4, 5). Based on the clinical success of
33 LNPs in delivering siRNAs to hepatic and non-hepatic targets (7–9), we explored if LNPs could
34 effectively deliver siRNA to neural cells. Neural cells are targets for drug delivery in multiple CNS
35 disorders such as Alzheimer's disease, Parkinson's disease, ischemic stroke, peripheral nerve
36 injuries, neuropathic and inflammatory pain (9–13). The key challenge associated with the delivery
37 of siRNA to neural cells are its poor accumulation and short duration of action inside cells.

38

39 The potent delivery characteristics of LNPs may allow them to be optimized for neural cell
40 delivery. LNPs are primarily composed of an ionizable cationic lipidoid along with helper lipids
41 like distearylphosphatidylcholine (DSPC), polyethylene glycol-dimyristoyl glycerol (PEG-DMG)
42 and cholesterol (13, 14). Ionizable cationic lipidoids allow higher encapsulation efficiencies and
43 greater intracellular release via effective endosomal escape (16). Ionizable cationic lipidoids with
44 pKa values between 6-7 acquire a positive charge at acidic pH and result in electrostatic
45 interactions with the negatively charged siRNA molecules leading to the spontaneous formation
46 of LNPs. At physiological pH of 7-7.4, these obtain a neutral charge and thereby largely eliminate

47 the toxicity associated with cationic lipids such as lipofectamine (17). This key feature renders the
48 LNPs a superior safety profile compared to cationic transfection agents. The acidic
49 microenvironment of endosomes lend the LNPs a positive charge because of which they associate
50 with negative anionic endosomal lipids leading to endosomal destabilization and improved siRNA
51 release into the cytoplasm (17, 18).
52
53 Seminal studies by Langer, Anderson and colleagues developed high throughput lipidoid
54 libraries consisting of thousands of ionizable cationic lipidoids and identified lead lipidoids based
55 on their *in vitro* and *in vivo* delivery efficacies in rodents as well as non-human primates. Amongst
56 those, C12-200 lipidoid demonstrated the highest knockdown and uptake *in vitro* (7, 19, 20).
57 Therefore, we chose C12-200 lipidoid as the ionizable cationic lipidoid component of LNPs. LNP-
58 based siRNA delivery harnesses several key advantages of LNP chemistry such as high
59 transfection efficiency, low toxicity and immunogenicity, protection of the payload from
60 physiological enzymes to increase their metabolic stability, ability for ligand conjugation and
61 enhancing the overall pharmacokinetics of the delivered cargo (22–24). The novelty of our work
62 lies in exploiting some of these cardinal features of LNPs to maximize siRNA uptake into neural
63 cells, a notoriously challenging delivery target.
64
65 In this pilot study, we formulated siRNA-LNPs using C12-200 lipidoid and characterized their
66 colloidal stability using dynamic light scattering. We characterized their cytocompatibility with a
67 panel of breast cancer cell lines and a model of sensory neurons, primary dorsal root ganglion
68 cultures. We studied the qualitative and quantitative uptake of siRNA delivered via LNPs into
69 neurons using fluorescence microcopy and flow cytometry, respectively. Despite mediating

70 similar levels of siRNA uptake, we found that LNPs are a safe carrier and show no signs of toxicity
71 in the neuronal models compared to the commercially available cationic lipid, Lipofectamine.
72 These findings encourage the further optimization of LNPs for knockdown of therapeutically-
73 relevant neuronal targets.
74

75 **Experimental section**

76 **Materials**

77 1,2-distearoyl-sn-glycero-3-phosphocholine (DSPC) (850365P) and 1,2-Dimyristoyl-rac–glycero-
78 3-methoxypolyethylene glycol-2000 (PEG-DMG) (8801518) were obtained from Avanti Polar
79 Lipids (Alabaster, AL). Cholesterol (8667) and Cy5-labeled siRNA were procured from Sigma-
80 Aldrich (St. Louis, MO). 1,1‘-((2-(4-(2-((2-(bis (2 hydroxy dodecyl) amino) ethyl)
81 (2hydroxydodecyl) amino) ethyl) piperazin1yl) ethyl) azanediyl) bis(dodecan-2-ol) (C12-200), an
82 ionizable cationic lipidoid was a generous gift from Alnylam Pharmaceuticals (Cambridge, MA).
83 Quant-iT Ribogreen RNA Assay Kit (R11490) was purchased from Life Technologies (Carlsbad,
84 CA). Triton X-100 was procured from Acros organics (Morris Plains, NJ). Heat-inactivated fetal
85 bovine serum (FBS) and phosphate buffered saline (PBS) were purchased from Hyclone
86 Laboratories (Logan, UT). TrypLE express, RPMI + GlutaMAX-I (1X) and DMEM/F-12 were
87 purchased from Life Technologies Corporation (Grand Island, NY). MCF-7, MDA-MB-231 and
88 BT-549 cell lines were generously provided by Dr. Jane Cavanaugh (Duquesne University).
89 Human cortical neuron cell line (HCN-2) (CRL-10742) and primary rat cortical neurons (RCN)
90 (A10840-02) were purchased from ATCC (Manassas, VA) and Thermo Fisher Scientific
91 (Frederick, MD) respectively. siGFP (AM4626), siGAPDH (Silencer Select GAPDH siRNA)
92 (4390849), siTRPV1 (5' GCGCAUCUUCUACUUCAACTT 3', 3'

93 TTCGCGUAGAAGAUGAAGUUG 5') [4390828 (Assay ID 554887)] and control, inverted
94 siTRPV1 (5' CAACUUCAUCUUCUACGCGTT 3', 3' TTGUUGAAGUAGAAGAUGCGC 5')
95 [4390828 (Assay ID 554886)] were procured from Thermo Fisher Scientific (Austin, TX). RNeasy
96 Mini Kit (74104) and QIAshredder (79654) were procured from Qiagen (Qiagen, Germantown,
97 MD). High-capacity cDNA Reverse Transcription Kit (4368813) was purchased from Thermo
98 Fisher Scientific (ThermoFisher, Waltham, MA). Forward (AAGGATGGAACAACGGGCTAG)
99 and reverse primers (TCCTGGTAGTGAAGATGTGGG) (299688565) for TRPV1 were procured
100 from Integrated DNA Technologies (Coralville, Iowa). All reagents were used as received unless
101 stated otherwise.
102
103 **Preparation of siRNA-loaded LNPs (siRNA-LNPs)**
104 LNPs were prepared using previously reported methods (8). Briefly, the ionizable cationic lipidoid
105 C12-200, DSPC, cholesterol and PEG-DMG were dissolved in ethanol at a molar ratio of
106 50/10/38.5/1.5. The concentrations and volumes used for LNP preparation are shown in **Table 1**.
107 A one mg/mL solution of siRNA was prepared in 10 mM citrate buffer, pH 4.0. The 'slow mixing'
108 and 'fast mixing' protocols are defined based on the speed used during the addition of the
109 lipid/ethanolic phase to the aqueous phase. For the 'slow mixing' method, the entire volume of the
110 lipid phase was added to the aqueous phase instantaneously (in a single shot) followed by vortexing
111 the mixture for 30 seconds while maintaining the Fisher benchtop vortexer knob at position '7'.
112 For the 'fast mixing' protocol, the lipid phase was added dropwise to the aqueous phase under
113 continuous vortexing for 30 seconds while maintaining the Fisher benchtop vortexer knob at
114 position '7'. A precalculated volume of 1*X* PBS pH 7.4 was then added to the LNPs to adjust the
115 final siRNA concentration to 400 nM. All the formulations were made at a final siRNA

116 concentration of 400 nM and cationic ionizable lipidoid/siRNA w/w ratio was maintained at 5:1,

117 unless stated otherwise.

118 **Table 1. Representative formulation scheme for LNPs**

Component	w/w% in final LNP mixture	Stock concentration (mg/mL)	Volume of the stock solution required (µL)
Ethanolic phase			
C12-200	50	1	12.5
Cholesterol	38.5	1	3.1
PEG-DMG	1.5	0.5	13.6
DSPC	10	0.5	16.9
Ethanol	-	-	78.9
	Total ethanolic phase volume		125
Aqueous phase			
siRNA	400 nM	1	2.5
10 nM citrate buffer	-	-	122.5
PBS	-	-	250
	Total aqueous phase volume		375
Final volume of LNPs prepared (µL)			500

119

120 **Agarose gel electrophoresis**

121 Agarose gel electrophoresis was performed to qualitatively confirm the encapsulation of siRNA

122 in LNPs. Briefly, a 2% agarose gel was prepared in 1*X* Tris-borate buffer composed of 108 g Tris

123 and 55 g Boric acid dissolved in 900 ml distilled water with 40 ml of 0.5 M Na_2EDTA and 0.05%

124 Ethidium bromide. Samples pre-mixed with 1*X* RNA loading buffer were electrophoresed in an

125 Owl EasyCast B2 Mini Gel Electrophoresis System (Thermo Fisher Scientific, St. Louis, MO) for

126 90 min. The gel was imaged under UV light using a Gel Doc system (ProteinSimple, San Jose,

127 CA).

128

129 **Determination of the extent of siRNA loading using the RiboGreen assay**

130 The extent of siRNA loading in the prepared LNPs was measured using the Quant-iT Ribogreen
131 RNA Assay Kit by following the manufacturer's instructions. RiboGreen is a fluorescent dye,
132 which, in its free form exhibits minimal fluorescence but when bound to a nucleic acid, it
133 fluoresces with an exceptionally high intensity that is directly proportional to the amount of nucleic
134 acid (25). Total siRNA content is defined as the amount of encapsulated and non-encapsulated/free
135 siRNA in the LNPs. The difference between the total and free siRNA was used to calculate the
136 amount of siRNA encapsulated within the LNPs. A fresh sample of two µg/mL dsRNA stock
137 solution was prepared each time with 1*X* Tris-EDTA (TE) and the standard curve was generated
138 at concentrations ranging from 0-1000 ng/mL. A free siRNA sample was prepared with 1*X* TE and
139 LNPs were lysed with 2% Triton X-100 in 1*X* TE to measure the "total" siRNA content. The
140 fluorescence intensities were measured on a SYNERGY HTX multi-mode reader (Winooski, VT)
141 at an excitation wavelength of 485 nm and an emission wavelength of 528 nm. The %
142 encapsulation efficiency was calculated using the **Eq. 1**.

143 $$\% \, siRNA \; encapsulation \; efficiency =$$

144 $$\frac{(Amount \; of \; total \; siRNA \; in \; the \; sample - Amount \; of \; free \; siRNA \; in \; the \; sample)}{Amount \; of \; total \; siRNA \; in \; the \; sample} \times 100\% \quad \textbf{Equation 1}$$

145

146 **Dynamic Light Scattering**

147 To determine the physical stability of LNPs, the average particle diameters, polydispersity indices
148 and zeta potentials of the blank and siGFP-loaded LNPs were measured by dynamic light
149 scattering (DLS) using a Malvern Zetasizer Pro (Malvern Panalytical Inc., Westborough, PA) over
150 a period of seven days with intermittent storage at 2-8°C and upon storage at 37°C for 24 h. We
151 also performed the colloidal stability analysis of LNPs 24 h post-preparation in 1*X* PBS and in

152 samples supplemented with FBS (10%) to determine its serum stability. The prepared LNPs were
153 diluted to a siRNA concentration of 40 nM using 10 mM 1*X* PBS pH 7.4 for particle size
154 measurements and using deionized water for zeta potential measurements. All measurements were
155 carried out in triplicate and the data are presented as average + standard deviation (SD) and are
156 representative of at least five-six independent experiments (measurement errors <5%).
157
158 **Cell culture**
159 MCF-7 and BT-549 cells were maintained in RPMI + GlutaMAX (1*X*) supplemented with 10%
160 FBS. MDA-MB-231 cells were maintained in DMEM/F-12 1:1 medium supplemented with 2.5
161 mM L-Glutamine + 15 mM HEPES Buffer + 110 mg/L Sodium Pyruvate + 10% FBS. The growth
162 medium was changed every 48 hours. Primary rat dorsal root ganglion (DRG) cultures were
163 isolated using previously reported methods (26). DRG cultures were maintained in DMEM/high
164 glucose (4.5 g/L glucose) media supplemented with 2.5 mM L-Glutamine + 15 mM HEPES Buffer
165 + 110 mg/L Sodium Pyruvate + 10 % FBS. Human cortical neuron cell line was maintained in
166 DMEM/high Glucose (4.5 g/L glucose) medium supplemented with 10 % FBS. Primary rat cortical
167 neurons were maintained in Neurobasal Plus medium supplemented with 200 mM GlutaMAX I
168 and B-27 Plus supplement. All cultures were maintained in a humidified incubator at 37 ºC and
169 5% CO_2.
170
171 **Cytocompatibility of LNPs**
172 MCF-7, MDA-MB-231, BT-549 cells and primary rat DRG neurons were seeded in a clear, flat
173 bottom Poly-D-Lysine coated 96-well plate (Azer Scientific, Morgantown, PA) for the
174 cytocompatibility studies. MCF-7, MDA-MB-231, BT-549 cells were seeded at a density of 5,000

175 cells/well and DRG neurons were seeded at a density of 1,500 cells/well. Untreated cells were
176 used as a control in all studies. Cells were transfected for 4 h with LNPs containing 50 nM of
177 siRNA in complete growth medium in a volume of 50 µL/well. We also treated cells with
178 increasing doses of siRNA-LNPs (10, 25, 50, 75 and 100 nM siGFP-loaded LNPs) to determine
179 any possible effects of dose escalation on cytocompatibility. Post-transfection, the transfection
180 mixture was replaced with 200 µL of fresh complete growth medium/well followed by a 24-hour
181 incubation at 37°C and 5% CO_2. The relative intracellular ATP levels were measured using the
182 Cell Titer-Glo luminescence assay (ATP assay) 24 h-post transfection using previously described
183 methods (27–29). The levels of ATP directly correlate with the cell numbers used here as a
184 measure of cell viability. The ATP levels of the treatment groups were measured against those of
185 the untreated or control cells. Briefly, 60 µL of the complete growth media and 60 µL of Cell Titer
186 Glo 2.0 reagent were added to each well of the 96-well plate. The plate was incubated for 15
187 minutes in dark at room temperature in an incubator-shaker (Thermo Fisher Scientific, Waltham,
188 MA). Following incubation, 60 µL of the mixture from each well was transferred to a flat-bottom,
189 white opaque 96-well plate (Azer Scientific, Morgantown, PA). The luminescence was measured
190 using SYNERGY HTX multi-mode reader (BioTek Instruments, Winooski, VT). Relative ATP
191 levels (%) were calculated for the transfection groups by normalizing them to the luminescence of
192 the untreated cells as shown in **Eq.2**.

193 $$\text{Relative ATP levels (\%)} = \frac{Luminescence\ from\ cells\ treated\ with\ samples}{Luminescence\ from\ untreated\ cells} \times 100 \qquad \textbf{Equation 2}$$

194

195 **Cy5 siRNA uptake into primary rat cortical neurons using flow cytometry**

196 Neurons were plated in a clear, flat-bottom Poly-D-Lysine coated 24-well plate (Genesee
197 Scientific, San Diego, CA) at a density of 50,000 neurons/well in Complete Neurobasal Plus media

198 and were allowed to acclimatize at 37°C and 5 % CO_2 for 4-5 days. Cy5 siRNA containing LNPs
199 were prepared as described earlier and diluted with the Complete Neurobasal Plus to a final Cy5
200 siRNA concentration of 50 nM. The neurons were incubated with the transfection mixture for 24
201 h. The transfection mixture contained either naked Cy5 siRNA or Cy5 siRNA-LNPs with PEG-
202 DMG (+ PEG-DMG) or Cy5 siRNA-LNPs without PEG-DMG (- PEG-DMG) or Cy5 siRNA-
203 Lipofectamine RNAiMAX complexes. Post-exposure, cells were gently removed from the wells
204 and collected in microcentrifuge tubes. The cell suspension was centrifuged at 300 g for 5 minutes
205 and the pellet was resuspended in 500 µL *1X* PBS. Cells were then analyzed using Attune NxT
206 Acoustic Focusing Cytometer (Singapore) equipped with Attune NxT software. The fluorescence
207 intensity of Cy5 siRNA was detected at an excitation wavelength of 638 nm and an emission
208 wavelength of 720/30 nm. A total of 30,000 events were recorded for each sample. Histogram
209 plots were obtained from the Attune NxT software. Cells were gated using forward vs. side scatter
210 plots to exclude dead cells and cell debris. Untreated cells were used as negative-staining controls
211 to set a gate for Cy5-negative and Cy5-positive populations. Data are presented as a percentage of
212 Cy5-positive (Cy5 (+)) events.
213
214 **Cy5 siRNA uptake by fluorescence microscopy in a human cortical neuron cell line**
215 We used fluorescence microscopy to determine the Cy5 siRNA uptake into a neuronal cell line.
216 Human cortical neurons (HCN-2) were seeded in a clear, flat-bottom, Poly-D-Lysine coated 48-
217 well plate (Genesee Scientific, San Diego, CA) at a density of 7,000 cells/well. The cells were
218 cultured in complete growth medium in a humidified incubator at 37°C and 5 % CO_2 for 1-2 weeks
219 while replenishing the growth medium every other day. After 4-5 days of culturing, the media was
220 replaced with 175 µL of the transfection mixture. The transfection mixture consisted of either Cy5

221 siRNA-LNPs or Cy5 siRNA-Lipofectamine RNAiMAX complexes containing 50 nM or 100 nM
222 of Cy5 siRNA or naked Cy5 siRNA diluted in complete growth media. Cells were incubated with
223 the transfection mixture for two, four and 24 hours at 37°C and 5% CO_2. After the respective time
224 points, the cells were washed once using pre-warmed PBS before adding 0.5 mL of the complete,
225 phenol red-free growth medium/well. Untreated cells and cells treated with Cy5 siRNA-
226 Lipofectamine RNAiMAX complexes were used as negative and positive controls, respectively.
227 Cells were imaged using an Olympus IX 73 epifluorescent inverted microscope (Olympus, Center
228 Valley, PA) to detect Cy5 signals at excitation and emission wavelengths of 651 nm and 670 nm,
229 respectively.
230
231 **Transfection of siTRPV1-LNPs in primary rat DRG neurons**
232 Primary rat DRG neurons were seeded in a clear, flat bottom Poly-D-Lysine coated 48-well plate
233 (Azer Scientific, Morgantown, PA) at a density of 2,500 cells/well in triplicates. The cells were
234 cultured in complete growth medium in a humidified incubator at 37°C and 5 % CO_2 for 48 hours.
235 Forty-eight hours post-seeding, the medium was replaced with 200 µL of the transfection mixture.
236 Cells were transfected with either 50 nM naked siTRPV1, LNPs containing 50 nM of siTRPV1 or
237 inverted siTRPV1 diluted in complete growth medium. Untreated cells and cells treated with
238 RNAiMAX lipofectamine/siTRPV1 complexes were used as negative and positive controls,
239 respectively. Cells were incubated with the transfection mixture for about eight-nine hours at 37°C
240 and 5 % CO_2. Post eight-nine hours of transfection, growth medium was added to bring up the
241 volume 0.5 mL/well followed by a 24-hour incubation.
242
243 **Quantitative reverse transcription PCR**

244 Twenty-four hours-post transfection, the medium was removed, and cells were washed with 1*X*
245 PBS and detached with TrypLE express. Detached cells were collected in microcentrifuge tubes
246 and washed with 1*X* PBS. Total RNA extraction and purification from the cells was done using
247 RNeasy Mini Kit and QIAshredder according to the manufacturer's instructions. The isolated RNA
248 was eluted in 30 µl of RNase-free water and stored at -80°C. The concentration of RNA was
249 measured using NanoDrop ND-1000 spectrophotometer (Waltham, MA). Briefly, 1.5 µl of the
250 sample was placed on the sample holder. The concentration (ng/µl) and the absorbance ratio of
251 260/280 were representative of the quantity and quality of the RNA, respectively. A 260/280 ratio
252 of ~2.0 was considered as "pure" for RNA. For mRNA detection, 2 µg of the RNA samples was
253 reverse transcribed into cDNA in technical triplicates using a high-capacity cDNA Reverse
254 Transcription Kit. All steps were done on ice to maintain integrity of the samples. Reverse
255 transcription was done by a two-step protocol according to the manufacturer's instructions. A
256 DNA Thermal Cycler (Perkin Elmer Cetus) was used to incubate the samples. The resulting cDNA
257 was diluted 10*X* with DEPC-treated water and stored at -20°C. Concentration of the cDNA was
258 measured using NanoDrop ND-1000. One µg cDNA was used to perform RT-qPCR using TaqMan
259 Gene Expression Master Mix and TaqMan Assays. An appropriate volume of the Gene Expression
260 Master Mix and TaqMan primers were added to get a total volume of 20 µL. Reactions were
261 performed in three technical replicates. The plate was covered with Microamp optical adhesive
262 film and RT-qPCR was done using a Stratagene Mx3000P.

263 **Statistical analysis**

264 The data is expressed as mean ± standard deviation (SD), wherever applicable. Comparative
265 statistical analyses were performed using either one-way, two-way ANOVA or One sample t and

266 Wilcoxon tests using GraphPad Prism 9 (GraphPad Software, San Diego, CA). Bonferroni's
267 multiple comparisons test was performed for comparative analyses using one-way ANOVA,
268 wherever applicable. Tukey's and Šídák's multiple comparisons tests for statistical comparisons
269 were performed using two-way ANOVA, wherever applicable. Alpha was set at 0.05.

270

271 **Results**

272 **Determination of the extent of siRNA loading using the**
273 **RiboGreen assay**

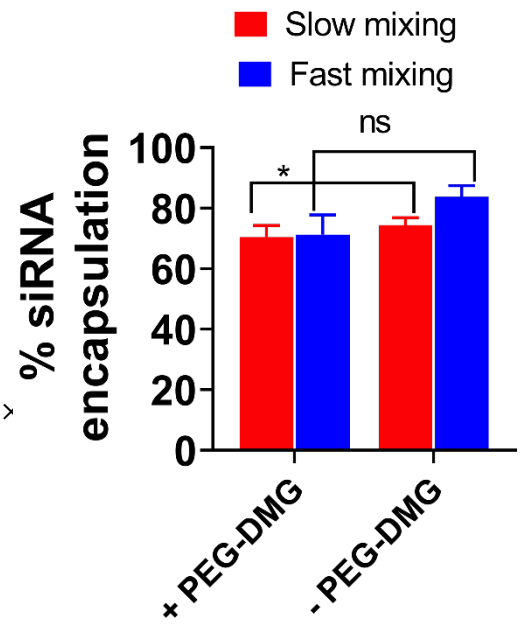

Figure 1. **Extent of siRNA encapsulation in LNPs prepared at different mixing speeds determined by the Ribogreen assay**. The extent of siRNA encapsulation in LNPs (+/- PEG-DMG) was calculated using the following equation

$$\left(\frac{(Amount\ of\ total\ siRNA\ in\ the\ sample - Amount\ of\ free\ siRNA\ in\ the\ sample)}{Amount\ of\ total\ siRNA\ in\ the\ sample}\right) \times 100\%$$

). SiRNA-LNPs were initially prepared in 10 mM citrate buffer and further diluted to a final siRNA concentration of 50 nM using 1*x* PBS. Data are presented as mean ± SD of n=3 samples. Statistical comparisons were made using two-way ANOVA. *$p < 0.05$ and ns: non-significant.

274

275 We used the Ribogreen assay as a quantitative measure to determine the extent of siRNA
276 encapsulation within the LNPs ***(Figure 1)*** and used agarose gel electrophoresis as a qualitative
277 tool to confirm the absence of 'free' or unentrapped siRNA **(*Supplementary Figure 1*)**. Triton X-
278 100 was used to lyse the LNPs resulting in the extraction of the entrapped siRNA to measure the
279 'total' siRNA (Total siRNA = entrapped siRNA + free siRNA). Fluorescence readout from LNPs
280 not treated with Triton X-100 is indicative of the amount of free siRNA. Two different mixing
281 speeds used during LNP formulation, slow *vs*. fast, were compared for determining their effects
282 on % siRNA encapsulation. The values increased from 74.4% at slow mixing to 83.8% at faster
283 mixing speeds for LNPs prepared without the inclusion of PEG-DMG, whereas we did not observe

284 a significant increase in siRNA loading for LNPs prepared with PEG-DMG at the different mixing
285 speeds.
286
287 **Colloidal stability of siRNA-loaded LNPs**
288
289 Physicochemical characteristics of nanocarriers such as particle diameter, polydispersity index
290 (PDI) and surface charge (zeta potential) are influential determinants of their biological activity
291 (30–32). Published studies have reported significant effects of physicochemical characteristics of
292 nano-sized systems on the overall delivery efficacy (33–36). Particle characteristics of self-
293 assembled systems such as LNPs can vary over time during storage potentially affecting their
294 biological activity. We also anticipated that neural cells may show a slower rate of particle uptake
295 compared to non-neuronal cells owing to limited endocytosis/other uptake pathways. We therefore
296 measured the changes in particle diameters and zeta potentials of the LNPs over a period of seven
297 days where the samples were refrigerated interim. Surface coating of nanoparticles using PEG-
298 DMG has been reported to improve their pharmacokinetic profile by reducing the recognition by
299 the mononuclear phagocyte system (37–39). We studied the effect of PEG-DMG in stabilizing
300 LNPs by comparing LNPs prepared in the presence (+) and absence (-) of PEG-DMG. We
301 compared the particle parameters of blank LNPs and siRNA-loaded LNPs to study the effect of
302 siRNA encapsulation on the resulting particle characteristics.
303
304
305
306
307

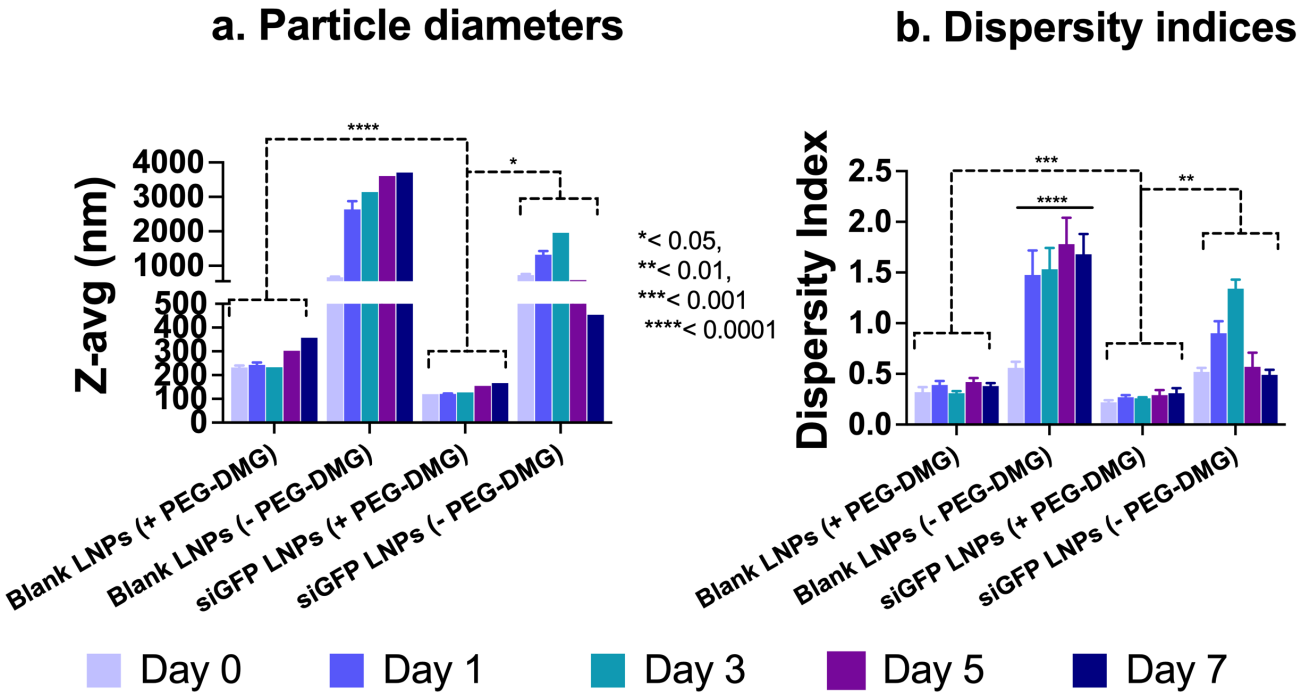

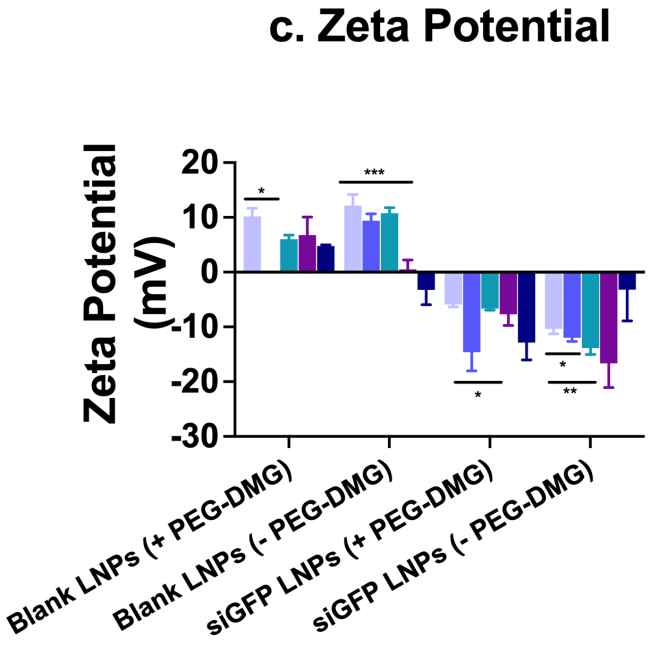

Figure 2. Colloidal stability of blank or siGFP-loaded LNPs measured using dynamic light scattering. SiGFP-LNPs were initially prepared in 10 mM citrate buffer and further diluted to a final siRNA concentration of 50 nM using 1*x* PBS (pH 7.4). The samples were stored at 2-8 ^{o}C while not in use. Z-average particle diameters (a), dispersity indices (b) and zeta potentials (c) were measured on a Malvern Zetasizer Pro. Data are presented as mean ± SD of n=3 measurements. Statistical comparisons were made using one-way ANOVA or One sample *t* and Wilcoxon tests. *$p < 0.05$, **$p < 0.01$, ***$p < 0.001$ and ****$p < 0.0001$.

330 Blank LNPs (+PEG-DMG) showed average particle diameters of about 250 nm which
331 increased to about 350 nm on day seven. In contrast, the diameters of LNPs (-PEG-DMG) were
332 about 900 nm post-preparation and increased to 4 µm after seven days ***(Figure 2a)***. A similar trend
333 was observed for the PDI values of blank LNPs i.e., an initial PDI of 0.32 increased to 0.4 after
334 seven days for LNPs (+PEG-DMG) and an initial PDI of 0.5 increased to 1.8 after seven days for
335 LNPs (-PEG-DMG) ***(Figure 2b)***. We observed a few statistically significant changes in the particle
336 diameters, PDI values and zeta potential of the prepared LNPs over the period of 7-days
337 ***(Supplementary Table 1)***. The narrow polydispersity indices and smaller average particle
338 diameters demonstrate the stabilizing effect of PEG-DMG in the LNPs. siGFP-loaded LNPs (with
339 PEG-DMG) showed average particle diameters of about 120 nm which increased to about 200 nm
340 on day seven ***(Figure 2a)***. Their initial PDI values of ca. 0.2 increased to about 0.3 after seven
341 days ***(Figure 2b)***. From this observation we can infer that siRNA loading in the LNPs results in
342 an additional stabilizing effect to the respective blank LNP counterparts resulting in narrow and
343 consistent PDI values and particle diameters.
344
345 The cationic lipidoid, C12-200, in the LNPs resulted in a net positive charge to the blank LNPs.
346 Blank LNPs containing PEG-DMG showed slightly lower zeta values (6-10 mV) compared to
347 blank LNPs without PEG-DMG (9-12 mV) **(*Figure 2c*)** that is likely explained by the insertion of
348 PEG chains in between the C12-200 lipidoids or due to formation of a PEG monolayer around
349 C12-200 (40). As seen from ***Figure 2*c**, siGFP-loaded LNPs showed a negative zeta potential
350 compared to their blank LNP counterparts. Although the changes were not statistically significant,
351 the zeta potentials of the siGFP-loaded LNPs decreased over the seven-day period from -5.91 mV
352 to -19.12 mV. Overall, the average particle diameters and polydispersity indices do not vary

significantly over a period of seven days. However, zeta potential values of siGFP-LNPs decreased over a period of seven days. Despite the apparent numerical differences in the zeta potentials, a one-way ANOVA analysis revealed that the differences were not significant.

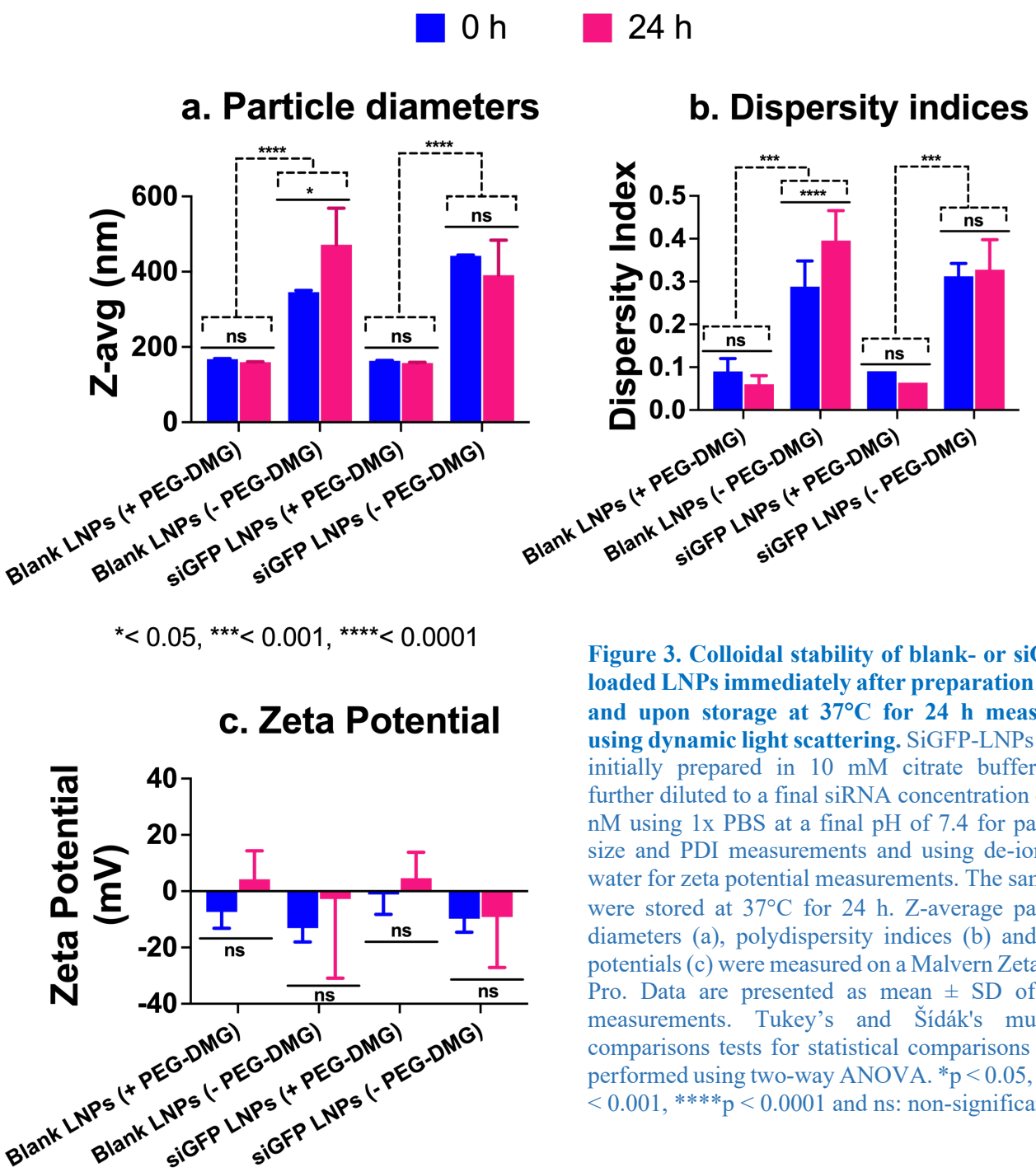

Figure 3. Colloidal stability of blank- or siGFP-loaded LNPs immediately after preparation (0 h) and upon storage at 37°C for 24 h measured using dynamic light scattering. SiGFP-LNPs were initially prepared in 10 mM citrate buffer and further diluted to a final siRNA concentration of 50 nM using 1x PBS at a final pH of 7.4 for particle size and PDI measurements and using de-ionized water for zeta potential measurements. The samples were stored at 37°C for 24 h. Z-average particle diameters (a), polydispersity indices (b) and zeta potentials (c) were measured on a Malvern Zetasizer Pro. Data are presented as mean ± SD of n=3 measurements. Tukey's and Šídák's multiple comparisons tests for statistical comparisons were performed using two-way ANOVA. *$p < 0.05$, ***$p < 0.001$, ****$p < 0.0001$ and ns: non-significant.

375 The colloidal stability of siGFP loaded- and blank LNPs was measured using dynamic light
376 scattering at 0 (immediately after preparation) and 24 h post-preparation upon storage at 37°C
377 (***Figure 3***). We also studied the effect of PEG-DMG in stabilizing LNPs by preparing LNPs with
378 (+) and without (-) PEG-DMG. Blank LNPs (+PEG-DMG) showed an average particle diameter
379 of about 167.8 nm that shifted to about 159.8 nm 24 h-post storage at 37°C. In contrast, the
380 diameters of LNPs (-PEG-DMG) were about 345.5 nm post-preparation and increased to 471.1
381 nm post 24 h storage at 37°C (***Figure 3a***). A similar trend was observed for the PDI values of
382 blank LNPs i.e., an initial PDI of 0.09 decreased to 0.06 for LNPs (+PEG-DMG) and an initial
383 PDI of 0.3 increased to 0.4 for LNPs (-PEG-DMG) 24 h-post storage at 37°C (***Figure 3b***). We
384 found a similar trend for the particle diameters and dispersity indices of siGFP-loaded LNPs, both
385 (+) and (-) PEG-DMG, 24 h-post storage at 37°C (***Figure 3a and b***). siGFP-loaded LNPs (+PEG-
386 DMG) showed an average particle diameter of about 163.2 nm that shifted to about 157.2 nm 24
387 h-post storage at 37°C. In contrast, the diameters of LNPs (-PEG-DMG) were about 442.2 nm
388 post-preparation and decreased to 390.7 nm 24 h-post storage at 37°C (***Figure 3a***). For the
389 dispersity indices, an initial value of 0.09 decreased to 0.06 for siGFP-loaded LNPs (+PEG-DMG)
390 and an initial value of 0.31 shifted to 0.32 for LNPs (-PEG-DMG) 24 h-post storage at 37°C
391 (***Figure 3b***). Nevertheless, the observed changes in particle diameters and dispersity indices of
392 blank LNPs (+ PEG-DMG) and siGFP-loaded LNPs (+ and – PEG-DMG) 24 h-post storage at
393 37°C were statistically insignificant. However, we noted a significant increase in the particle
394 diameters (*$p < 0.05$) and dispersity indices (****$p < 0.0001$) of blank LNPs (-PEG-DMG) likely
395 due to the absence of PEG-DMG and the siGFP cargo—that are known to provide a stabilizing
396 effect by inhibiting particle-particle aggregation and via complexation of the negatively charged

397 siRNA with the positively-charged C12-200, respectively. Noteworthy, we noted a similar trend
398 of the stabilizing effects of PEG-DMG and the siGFP cargo in ***Figure 2***.
399
400 Blank LNPs containing PEG-DMG showed slightly negative zeta potentials (-5 to -7 mV)
401 that shifted to slightly cationic values (3 to 4 mV) whereas the zeta potentials of blank LNPs
402 without PEG-DMG were about -13 mV that increased to about -2 mV 24 h-post storage at 37°C
403 **(*Figure 3c*)**. siGFP-loaded LNPs (+ PEG-DMG) showed a zeta potential of -1.2 mV that increased
404 to about 4.6 mV whereas the LNPs (- PEG-DMG) counterparts showed a zeta potential of -9.8 mV
405 that increased to about -9.1 mV 24 h-post storage at 37°C **(*Figure 3c*)**. Despite the apparent
406 numerical differences, it should be noted that the measured zeta potentials reflect electrostatically-
407 neutral samples and a two-way ANOVA analysis revealed that the differences were not significant.

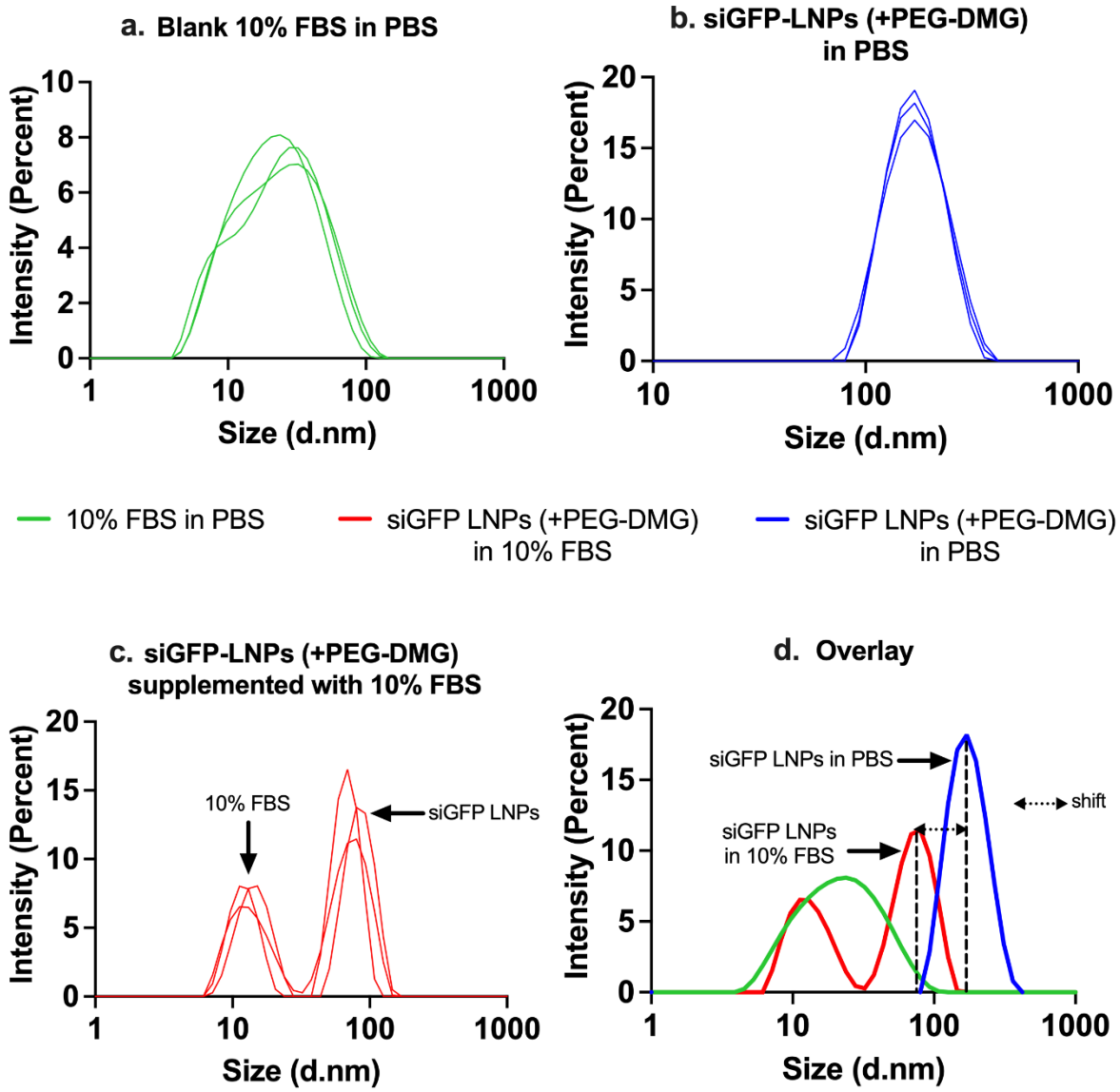

Figure 4. Intensity size distribution plots demonstrating the colloidal stability of siGFP-loaded LNPs (+PEG-DMG) supplemented with 10% FBS. (a) A blank sample consisting of 10% FBS in 1x PBS was used to understand the serum protein-mediated scattering. (b) SiGFP-LNPs (+PEG-DMG) were initially prepared in 10 mM citrate buffer and further diluted to a final siRNA concentration of 50 nM using 1x PBS. LNPs supplemented with 10% FBS were measured to determine their serum stability. (d) An overlay depicts the pattern of the size distribution obtained for all the LNP samples.

The particle diameters of siGFP-LNPs (+PEG-DMG) containing 10% FBS was measured using dynamic light scattering to determine the effect of serum proteins on the colloidal stability of LNPs. We specifically chose siGFP-LNPs (+PEG-DMG) to study the effect of serum since the

419 presence of siRNA and PEG-DMG resulted in the maximum stability of LNPs with respect to
420 particle diameters and dispersity indices **(Figure 2*a and b*)**. We first measured the particle
421 diameter of a control sample containing 10% FBS in PBS **(*Figure 4a*)** that showed an average
422 particle diameter of 19.6 nm whereas siGFP-LNPs (+PEG-DMG) in PBS showed an average
423 particle diameter of about 170 nm ***(Figure 4b)***. We observed distinct size distribution by intensity
424 peaks for the blank 10% FBS as well as LNP samples ***(Figure 4a and b)***. We then measured the
425 particle diameter of siGFP-LNPs (+PEG-DMG) that was supplemented with 10% FBS. ***Figure 4*c**
426 has two distinct peaks denoting peaks corresponding to 10% FBS and the siGFP-LNPs (+PEG-
427 DMG) at 20.2 nm and 80.5 nm respectively. The overlay size distribution plot demonstrated a
428 "shift" in the siGFP-LNPs (+PEG-DMG) peak towards the left (lower particle diameters) when
429 the LNPs were supplemented with 10% FBS as opposed to those in PBS (80.5 nm vs 170 nm)
430 **(*Figure 4d)***. We speculate that the observed decrease in diameter is suggestive of the additional
431 stabilizing effects of serum (10% FBS) on the LNP diameters. This, in fact, may be
432 beneficial/favorable for LNP uptake ***(Figure 7 and Figure 8)*** as neurons may preferentially
433 internalize smaller compared to larger LNPs.

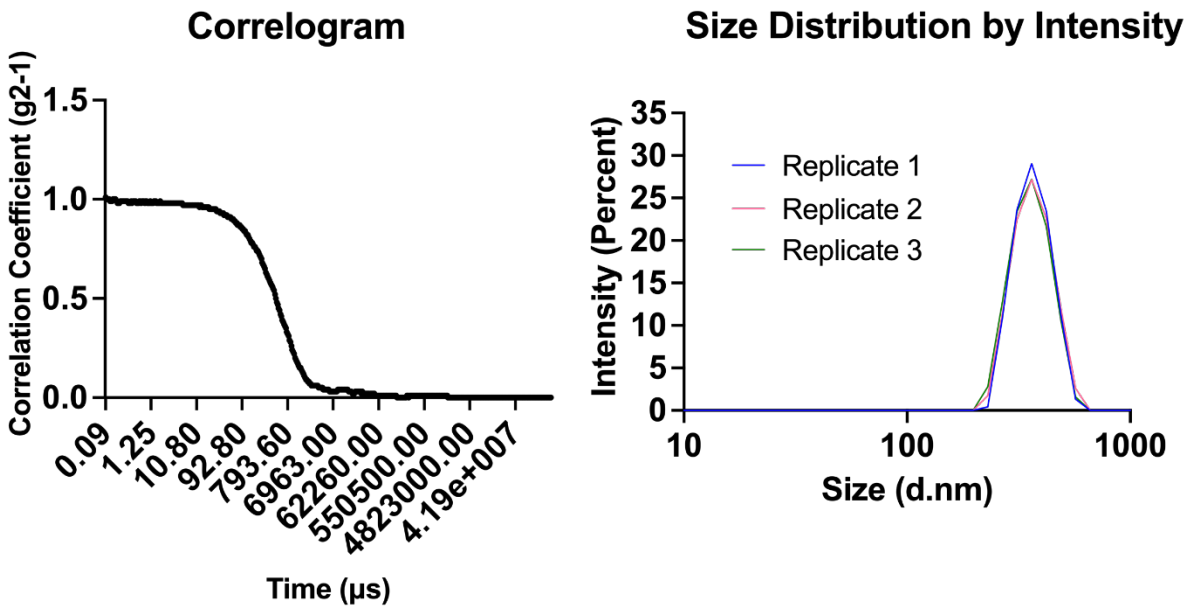

Figure 5. Representative correlogram and intensity size distribution plots of siGFP-loaded LNPs (+PEG-DMG). siGFP-LNPs were initially prepared in 10 mM citrate buffer and further diluted to a final siRNA concentration of 50 nM using 1*x* PBS at a final pH of 7.4 prior to particle size measurements on a Malvern Zetasizer Pro.

Table 2. Comparison of the Y-intercept in the autocorrelograms from the colloidal stability data (Figure 2) at different time points.

Groups	Y-intercept				
	Day 0	Day 1	Day 3	Day 5	Day 7
Blank LNPs (with PEG-DMG)	0.98	0.98	0.94	0.89	0.8
Blank LNPs (without PEG-DMG)	0.99	1.3	1	1	0.9
siGFP LNPs (with PEG-DMG)	0.96	0.93	0.9	0.86	0.87
siGFP LNPs (without PEG-DMG)	1	1.1	1.1	0.96	0.88

The correlation function is a statistical analysis tool for measuring the non-randomness in a data set that is depicted here as a correlogram. A correlogram is a plot of the correlation coefficient G (τ) vs time (µs) **(Figure 5)**. The Y-intercept of the correlogram is indicative of the signal to noise ratio and presence/absence of multiple scattering. A Y-intercept of ~0.9-1.15 indicates a good

signal in the absence of multiple scattering. Samples with multiple scattering show a Y-intercept of ~0.6-0.8 and samples with number fluctuations show a Y-intercept of ~1.15-1.4 (41). As observed from **Table 2**, the Y-intercept values for all the LNP groups over a period of seven days ranged from 0.8-1.1 that is indicative of a good signal-to-noise ratio in the absence of multiple scattering and number fluctuations.

Cytocompatibility of C12-200-LNPs

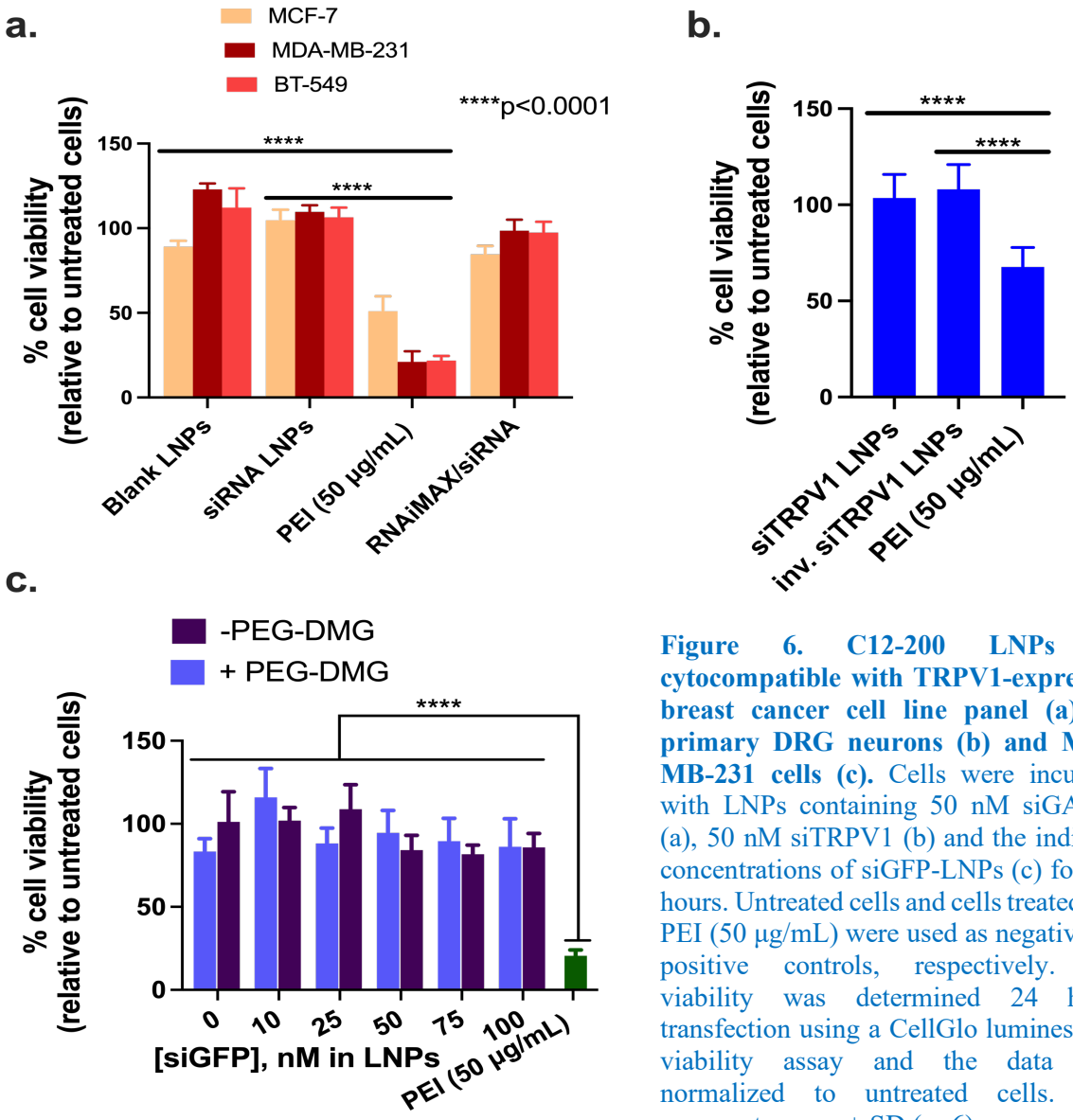

Figure 6. C12-200 LNPs are cytocompatible with TRPV1-expressing breast cancer cell line panel (a), rat primary DRG neurons (b) and MDA-MB-231 cells (c). Cells were incubated with LNPs containing 50 nM siGAPDH (a), 50 nM siTRPV1 (b) and the indicated concentrations of siGFP-LNPs (c) for four hours. Untreated cells and cells treated with PEI (50 µg/mL) were used as negative and positive controls, respectively. Cell viability was determined 24 h-post transfection using a CellGlo luminescence viability assay and the data were normalized to untreated cells. Data represents mean + SD (n=6).

469 We studied the cytocompatibility of the prepared C12-200/siGAPDH LNPs with MCF-7,
470 MDA-MB-231 and BT-549 cells as these cell models are known to overexpress TRPV1, a
471 neuronal target for siRNA delivery ***(Figure 6a)*** (42). We also studied the compatibility of C12-
472 200/siTRPV1 LNPs with primary rat dorsal root ganglion (DRG) neurons ***(Figure 6b)***. We
473 specifically chose primary rat DRG neurons due to their high expression of TRPV1 (41, 42).
474 TRPV1 is reported to be expressed in 60% of the peripheral nociceptors present in the DRG (45)
475 and is a potential neuronal target for gene knockdown. Cell Titer Glo assay (referred henceforth
476 as the ATP assay) was used the study cytocompatibility of LNPs. The ATP assay is a simple and
477 straightforward technique wherein the readout in relative luminescence units (RLU) can be directly
478 correlated with the ATP levels in the cells. RLU of the untreated cells were normalized to 100%
479 cell viability. Untreated cells and cells treated with a synthetic polycation, polyethyleneimine (PEI)
480 served as the negative and positive controls, respectively. As we expected, MCF-7, MDA-MB-
481 231, BT-549 cells and primary DRG neurons treated with PEI (50 µg/mL), a synthetic polycation
482 known to induce apoptosis showed a 50-60% reduction in cell viability (46). However, MCF-7,
483 MDA-MB-231 and BT-549 incubated with C12-200/siGAPDH LNPs showed very little evidence
484 of cell death, with cell viabilities >95% 24 h-post transfection ***(Figure 6a)***. Similarly, siTRPV1-
485 loaded C12-200 LNPs were well tolerated (cell viabilities of ca. 100%) by primary DRG neurons
486 ***(Figure 6b)***. We tested the effect of siRNA dose escalation by incubating MDA-MB-231 cells
487 with increasing concentrations of siRNA-LNPs (10, 25, 50, 75 and 100 nM siGFP-loaded LNPs).
488 We noticed cell viabilities >85% 24 h-post transfection **(*Figure 6c*)** suggesting that higher siRNA
489 and concomitant lipid doses were well-tolerated by the cells. There was a significant difference
490 ($p<0.0001$) in the % cell viabilities of cells treated with siRNA-LNPs compared to those treated
491 with the positive control, PEI (20% cell viability).

492

493 **Flow cytometry analysis of Cy5 siRNA uptake into primary rat cortical neurons**

494 After confirming that LNPs had little-to-no effect on cell viability, we next wanted to
495 determine if LNPs were taken up by neurons. Because of their commercial availability as well as
496 their non-mitotic nature similar to that of the primary rat DRG neurons, primary rat cortical
497 neurons were used to quantify the uptake levels of Cy5 siRNA using flow cytometry.
498 Lipofectamine RNAiMAX, a cationic lipid, was used as a positive control. Flow cytometry is a
499 quantitative tool for single-cell analysis to measure the light scattered and the fluorescence emitted
500 form a single cell (47). The dead cells/debris were likely removed at the centrifugation step during
501 the sample processing and as a result, we did not observe any dead cells or debris ***(Figure 7a, left)***
502 that are typically found at the bottom left corner of the SSC-A vs. FSC-A plot (48). We then
503 analyzed whether the cells were present in a monodisperse cell suspension to allow for single cell
504 analysis. The forward scatter distributions for height *vs*. area (FSC-A v/s FSC-H) showed a linear
505 profile for about 92% of the recorded events which indicated a single-cell suspension ***(Figure 7a,***
506 ***right)***. We analyzed untreated cells and gated out the auto fluorescence ***(Figure 7b, left)***. Thus, a
507 shift of signal to the right of the histogram gate (R1 region) was considered to signify that the cell
508 was Cy5-positive (+). The proportion of Cy5 (+) cells directly correspond to the % uptake of Cy5
509 siRNA in the neurons as represented by the individual histogram plots for the different groups
510 ***(Figure 7c)***.

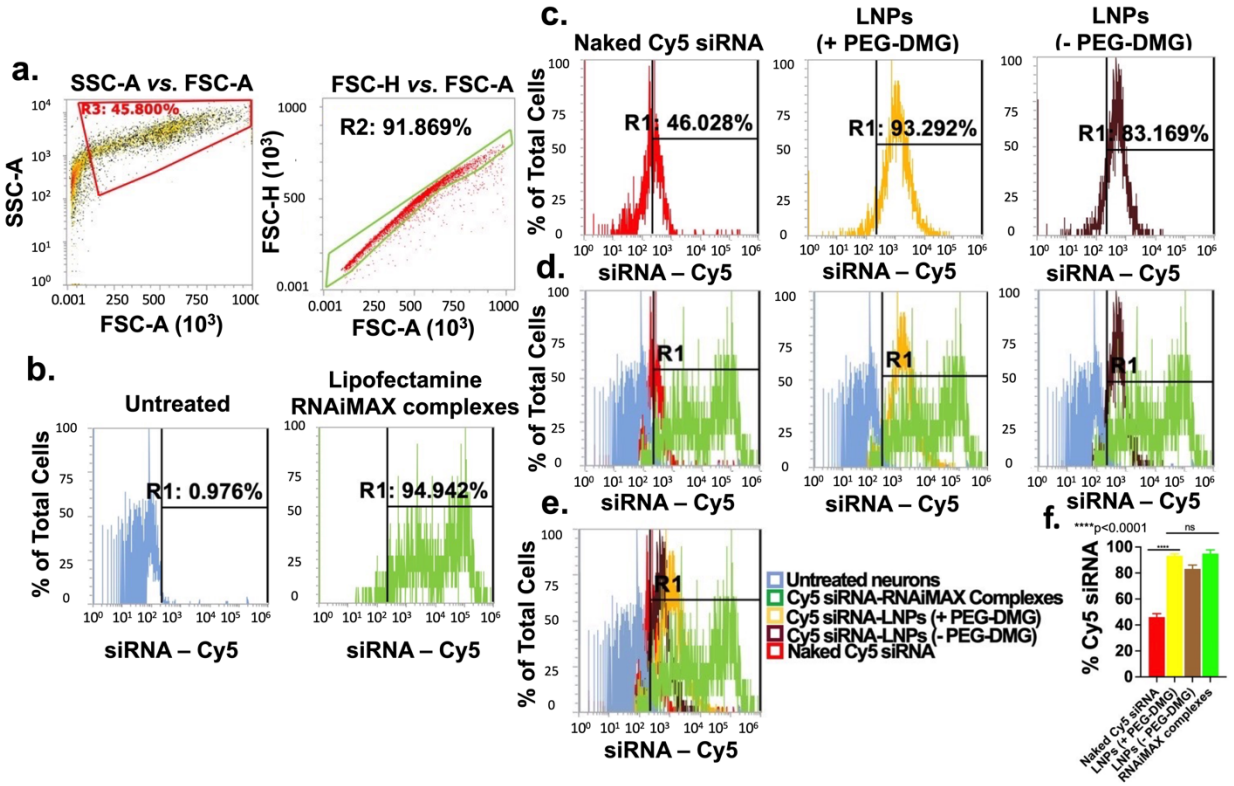

Figure 7. Uptake of LNPs into rat primary cortical neurons determined using flow cytometry analysis. Cells were transfected for 24 h with the indicated samples in a 24-well plate. Cy5 siRNA-Lipofectamine RNAiMAX complexes and untreated cells were used as positive and negative controls, respectively. Data are presented as percentages of positive cells for Cy5 (Cy5 (+)). SSC-A vs. FSC-A and FSC-H vs. FSC-A plots of untreated cells demonstrating monodispersed cells. (a), Untreated and Cy5 siRNA/Lipofectamine RNAiMAX-treated cells (b), Cells treated with the indicated samples (c), Overlay histograms comparing Cy5 (+) cells in each treatment group in comparison to the controls (d), Overlay histograms (e) and % Cy5 siRNA uptake by the neurons for the respective groups (f). The histograms are representative of quadruplicate samples. Statistical comparisons were made using one-way ANOVA. ****$p < 0.0001$.

We then analyzed the % uptake of Cy5 siRNA encapsulated in LNPs prepared with (+) and without (-) the inclusion of PEG-DMG. Around 92-94% ***(Figure 7c (yellow))*** and 81-83% ***(Figure 7c (brown))*** cells were Cy5 (+) when transfected with Cy5 siRNA-LNPs prepared with and without the inclusion of PEG-DMG, respectively. ***Figure 7*****d** shows the relative Cy5+ cells in each of the indicated groups in reference to the untreated (blue) and positive control-treated (green)

528 groups. The rightward shift in intensities of Cy5 (+) cells for all the groups in comparison with the
529 controls are demonstrated in the overlay histogram plot in ***Figure 7*****e**. As expected, the % uptake
530 of Cy5 siRNA was least in cells treated with free Cy5 siRNA and greatest in cells treated with
531 LNPs (+PEG-DEMG) and Cy5 siRNA/Lipofectamine RNAiMAX complexes ***(Figure 7e and f)***.
532 Furthermore, as seen in ***Figure 7*****e**, we saw a greater uptake of LNPs with PEG-DMG as compared
533 to those without PEG-DMG. Particle sizes of LNPs play one of the major roles in determining
534 uptake levels and therefore, lower diameter particles may allow efficient cellular internalization.
535 Furthermore, a significant difference in the uptake of Cy5 siRNA was observed when transfected
536 with naked Cy5 siRNA and Cy5 siRNA-LNPs (+/- PEG-DMG) ***(Figure 7e and f)***. This reiterates
537 the need for a safe and efficient transfection agent to maximize the uptake of siRNA in neurons, a
538 hard-to-transfect cell type.
539

540 Around 94-96% of the cells were Cy5 (+) for the Lipofectamine RNAiMAX group indicating
541 efficient uptake ***(Figure 7b right and f)***. Charge-based interactions of cationic lipids with
542 negatively-charged cells allows for higher uptake as compared to neutral or negatively-charged
543 particles. About 44-46% of the cells were Cy5 (+) for the naked Cy5 siRNA transfection group
544 ***(Figure 7c (red))***. The difference between the uptake mediated by LNPs (+ PEG-DMG) and
545 Lipofectamine RNAiMAX was statistically non-significant ***(Figure 7f)***. Despite the similar levels
546 of uptake among the LNP(+PEG-DMG) and lipofectamine groups, it must also be pointed out that
547 the uptake mediated by Lipofectamine RNAiMAX was accompanied with noticeable cell
548 stress/toxicity upon visual observation under a microscope whereas LNPs showed a superior safety
549 profile.

550

551 **Cy5 siRNA uptake by fluorescent microscopy in a human cortical neuron cell line**

552 We studied the effect of exposure time on the uptake of LNPs by incubating the cells for two,
553 four or 24 hours. PEGylation is known to regulate the uptake kinetics of LNPs into cells (49). We
554 compared the differences in uptake for LNPs prepared with/without PEG-DMG. Although
555 Lipofectamine RNAiMAX is a gold standard transfection agent for RNA molecules, it is also quite
556 toxic to cells owing to its strong cationic nature. Therefore, it was unsurprising when we saw
557 changes in morphology indicating cell death, just 2 h after Lipofectamine RNAiMAX was added
558 to cortical neurons, while untreated cells continued to appear spindle-shaped and healthy ***(Figure***
559 ***8a)***.

560

561 For this experiment, cells were incubated either with naked Cy5 siRNA, Cy5 siRNA LNP with
562 PEG-DMG, with Cy5 siRNA LNP without PEG-DMG, with Lipofectamine RNAiMAX Cy5
563 siRNA, or were left untreated. We qualitatively compared the fluorescence intensity among the
564 cells treated with the above samples. Cells treated with naked Cy5 siRNA showed less intense
565 fluorescent signals as compared to cells treated with Cy5 siRNA-LNPs (+/- PEG-DMG) for the
566 two- and four-hour incubation time points ***(Figure 8a, b)***. However, we saw a noticeable increase
567 in siRNA uptake 24 h-post transfection **(*Figure 8c*)**. The next pivotal observation was the
568 difference in uptake from the LNPs (+/- PEG-DMG) groups. As mentioned earlier, PEG-DMG
569 plays a key role in determining the physical stability of LNPs as it allows to maintain lower particle
570 diameters by inhibiting particle aggregation (38). We also noted time-dependent differences in
571 Cy5 siRNA uptake for the LNPs formulated with and without PEG-DMG. LNPs formulated with
572 PEG-DMG showed a time-dependent increase in the uptake of Cy5 siRNA as opposed to LNPs

573 without PEG-DMG where the extent of uptake was not time-dependent. We observed that only a
574 few cells did not show Cy5 siRNA signals when treated with Cy5 siRNA-LNPs (+ PEG-DMG)
575 two- and four-hours post-transfection whereas 24 h post-treatment almost all the cells showed
576 signals corresponding to Cy5 siRNA. Conversely, cells treated with Cy5 siRNA-LNPs (- PEG-
577 DMG) showed efficient uptake of Cy5 siRNA post two- and four hours transfection. A zoomed-
578 in image of cells treated with LNPs containing 50 nM Cy5 siRNA is presented in ***Figure 8*****d** to
579 show image resolution. This particularly depicts the uptake of Cy5 siRNA LNPs associated with
580 diffuse cytoplasmic fluorescence.

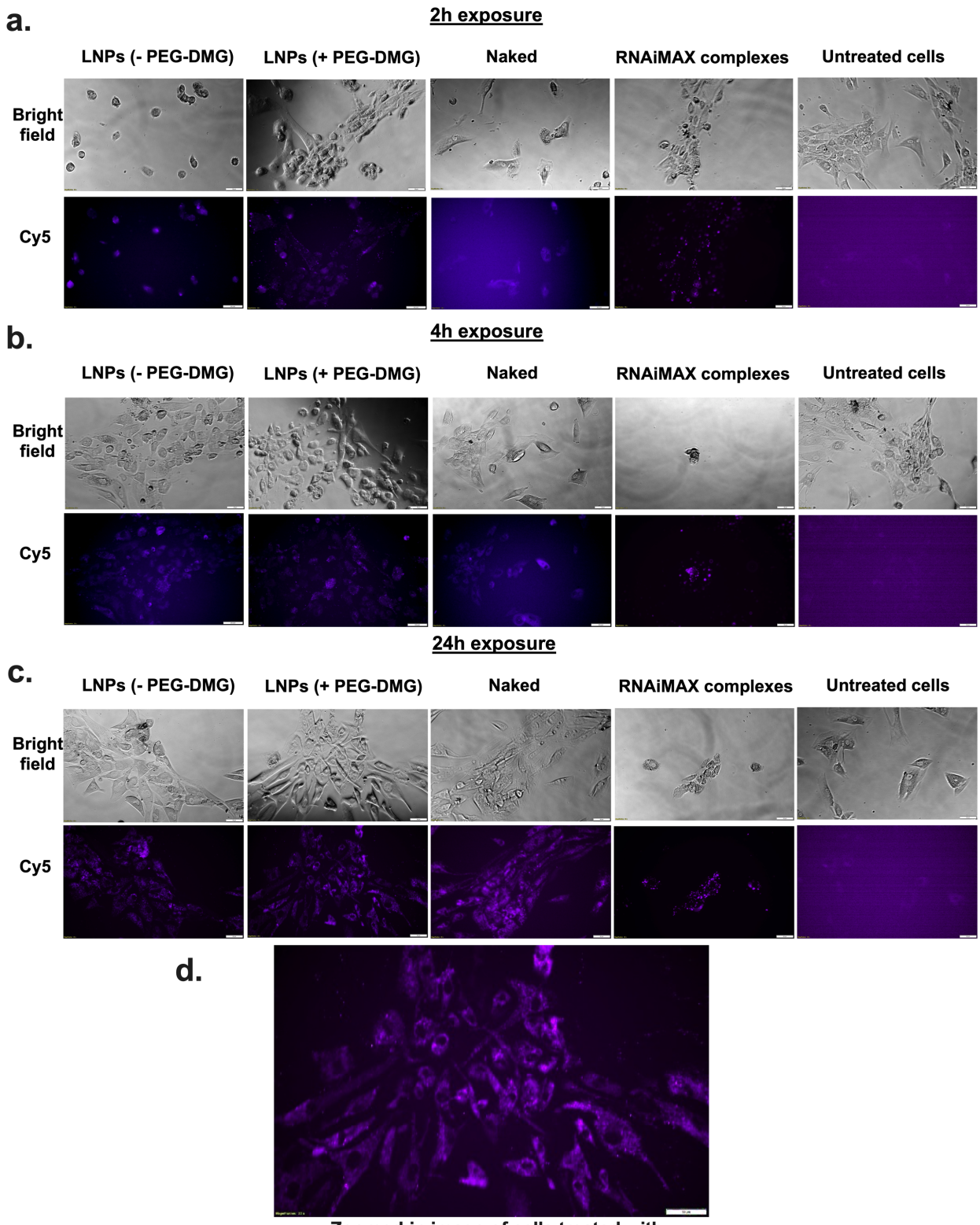

Zoomed-in image of cells treated with
Cy5 siRNA LNPs (+PEG-DMG) 24 h post-exposure

581

582 **Figure 8. Cellular uptake of Cy5 siRNA determined using fluorescent microscopy.** HCN-2
583 cells (human cortical neuron cell line) were incubated for 2 hours (a) 4 hours (b) and 24 hours (c)
584 with the indicated samples containing 50 nM Cy5 siRNA. Panel (d) represents the zoomed-in
585 image depicting HCN-2 cells incubated with LNPs with PEG-DMG. Scale bar = 50 µm. Cells
586 were imaged using an Olympus IX 73 epifluorescent inverted microscope to detect Cy5 signals at
587 excitation and emission wavelengths of 651 nm and 670 nm, respectively. Images are
588 representative of n=3 independent wells.
589

590

591 **Discussion**

592 The goal of this pilot study was to determine if LNPs based on the benchmark C12-200 lipidoid
593 can be used for siRNA transfection into neurons, a notoriously challenging yet clinically
594 unmet/interesting delivery target. We propose that the well-documented delivery advantages of
595 LNPs including their high levels of siRNA encapsulation, favorable pharmacokinetics, limited
596 immune activation, uptake into target cells and efficient endosomal escape for siRNA into the
597 cytoplasm (14, 47, 48) make them interesting candidates for neural delivery applications.

598

599 In this pilot study, we prepared and characterized C12-200 LNPs using DLS. The RiboGreen
600 assay is a well-validated quantitative method to determine the % siRNA loading in LNPs (49, 50).
601 Encapsulation of siRNA in the LNPs for the slow and fast mixing (without PEG-DMG) speeds
602 were about 74.4% and 83.8%, respectively. LNPs with and without PEG-DMG (for fast mixing
603 speed) showed encapsulation efficiencies of about 71.4 % and 83.8 %, respectively ***(Figure 1)***
604 which were comparable to the entrapment of siRNA reported for some of the top LNP candidates
605 (54). Although we did not find a significant difference in the encapsulation efficiencies of LNPs
606 prepared with and without PEG-DMG, the inclusion of PEG-DMG serves other vital roles *i.e.*,
607 maintaining lower particle diameters by inhibiting particle aggregation and providing a stealth
608 effect for longer circulation times *in vivo* (37, 38). We further studied the physicochemical stability

609 of the prepared LNPs and compared the stabilizing effect provided by the inclusion of PEG-DMG
610 and siRNA in the LNPs. We utilized siGFP as the model siRNA to compare the siRNA-loaded
611 and blank LNP counterparts prepared both with and without PEG-DMG. We observed a non-
612 significant increase or change in the particle diameters, polydispersity indices and zeta potential
613 over a one-week storage period at 2-8 °C for all the samples ***(*Figure 2*)***. Nevertheless, the particle
614 diameters differed significantly for blank *vs*. siRNA-loaded LNPs and LNPs with *vs*. LNPs without
615 PEG-DMG ***(*Figure 2*a)***. A similar trend was also observed for the polydispersity indices of blank
616 and siRNA-loaded LNPs; both with and without PEG-DMG ***(*Figure 2*b)***. Our data demonstrated
617 that both siRNA loading and PEG-DMG provided a stabilizing effect to the LNPs by maintaining
618 lower particle diameters and uniform dispersity indices over a period of seven-days. The
619 stabilizing effects of siRNA and PEG-DMG on the resulting particle diameters and dispersity
620 indices were noted when the LNPs were stored for 24 h at 37°C **(*Figure 3*)**. LNPs showed further
621 lower particle diameters (ca. 80.5 nm) when sizes were measured in the presence of serum (10%
622 FBS) suggestive of the additional serum-mediated stabilization **(*Figure 4*)**.
623
624 Although LNPs are deemed to be safe and are well-tolerated by most of the cells, determining
625 their safety and tolerability in neural cells was our primary aim. As shown in ***Figure 6***, LNPs
626 were deemed to be well-tolerated by primary DRG neurons as evident by >95% cell viabilities.
627 Increasing the dose of siRNA (and concomitantly the dose of the lipids) did not alter the safety
628 profile of LNPs ***(Figure 6c)***. Establishing the safety profile of LNPs with neural cells allowed
629 further evaluation of their uptake in neural cell lines. We studied the uptake of Cy5 siRNA-loaded
630 LNPs in primary rat cortical neurons and a human neuronal cell line using flow cytometry and
631 fluorescence microscopy, respectively. Previously, Howard *et al* and Thiramanas *et al.* studied the

632 cellular uptake of Cy5 siRNA using flow cytometry (52, 53). As PEG-DMG is known to stabilize
633 the LNPs with resulting lower particle diameters and thus have an impact on their cellular uptake,
634 we compared LNPs prepared with (+) and without (-) PEG-DMG. We used the siRNA complexes
635 of the cationic transfection agent, Lipofectamine RNAiMAX, as a positive control. The cell-
636 associated fluorescence (Cy5 (+) neurons) for the Cy5 siRNA-LNPs (+ PEG-DMG) group was
637 about 94%—2-fold greater than the neurons transfected with naked Cy5 siRNA group ***(*Figure 7*c,***
638 ***e, and f)***. As expected, despite its transfection-induced toxicity, Cy5 siRNA-Lipofectamine
639 RNAiMAX-treated cells demonstrated the highest proportion of Cy5 (+) cells ***(*Figure 7*c, e, and***
640 ***f)***. On the other hand, cells treated with LNPs appeared healthy and showed no visible signs of
641 toxicity, highlighting the safety of LNPs over cationic transfection agents like Lipofectamine
642 RNAiMAX. There was a significant difference in the uptake of neurons transfected with naked
643 Cy5 siRNA as compared to the neurons transfected with the LNPs (both with and without PEG-
644 DMG) emphasizing the need for an effective transfection agent for neural cell uptake ***(*Figure 7*f)***.
645

646 We also performed fluorescence microscopy to qualitatively study the uptake of Cy5 siRNA
647 into neural cells. A technical caveat of such qualitative assessments is rooted in the fact that the
648 observed/apparent fluorescent intensities are not normalized to cell number. The cells appeared to
649 be healthy, and spindle-shaped in all the treatment groups except for the Lipofectamine
650 RNAiMAX group where cells appeared stressed and rounded as early as at the 2 h timepoint
651 ***(Figure 8a)***. As described earlier, we speculate that this is due strong cationic nature of
652 Lipofectamine RNAiMAX. We did not observe a greater uptake for cells treated with LNPs at 100
653 nM siRNA concentration **(*Supplementary Figure 2)***. Nearly all the cells in the field showed Cy5
654 fluorescent signals 24 h-post exposure **(*Figure 8c)*** compared to the 2 and 4 h time points **(*Figure***

655 ***8a and b)***, suggesting that neural cells require a longer transfection time compared to non-neural
656 cells. LNPs formulated with PEG-DMG showed a time-dependent increase in the uptake of Cy5
657 siRNA as opposed to LNPs without PEG-DMG. The time dependent uptake of LNPs formulated
658 with PEG-DMG was in agreement with the PEG-DMG dissociation kinetics as predicted by Mui
659 *et al*. (57). The PEG-lipid component of the LNPs undergoes desorption from the surface of LNPs
660 which results in efficient uptake of the cargo into the cells (58). Studies have reported desorption
661 rates of PEG-DMG from the LNPs at a rate of 45%/h only after which LNPs were taken up by
662 cells (57). We observed a similar trend of Cy5 siRNA uptake when neurons were transfected with
663 LNPs (+ PEG-DMG). At the 2 and 4 h time points, most (but not all) of the cells had efficiently
664 taken up the LNPs. However, 24 h post-treatment, almost all the cells in the field of view showed
665 fluorescent puncta corresponding to Cy5 siRNA. In contrast, in cells transfected with Cy5 siRNA-
666 LNPs (- PEG-DMG), all the cells demonstrated complete and uniform uptake irrespective of the
667 incubation period. The effects of RNAiMAX-mediated toxicity were evident via altered cell
668 morphology seen in the phase contrast images.
669
670 Overall, both flow cytometry and fluorescent microscopy analysis in cortical neurons
671 demonstrated efficient uptake of siRNA delivered using LNPs in the absence of noticeable toxicity
672 while the cationic Lipofectamine RNAiMAX-mediated uptake was concomitant with significant
673 cellular toxicity. Based on these findings, we conclude that LNPs are a safe carrier for siRNA
674 delivery to neural cells. We are currently screening a pre-existing LNP library prepared using
675 different lipidoid chemistries to identify LNP candidates for safe and efficient neuronal gene
676 knockdown. We anticipate that the results of these studies will set the foundation for using LNPs
677 for neural cell transfection in a variety of CNS diseases. While our approach validates using LNPs

678 for uptake of siRNA into neural cells, their knockdown efficacy and therapeutic index remain an
679 open question which we are currently investigating.
680
681 **Conclusion**
682 SiRNA-loaded LNPs remained stable over a period of seven days and were well-tolerated by
683 neural cell models, allowing their further exploration for gene silencing. Although the LNPs are
684 comparable to Lipofectamine RNAiMAX in facilitating siRNA uptake into cortical neurons, the
685 ionizable cationic LNPs are safer and well-tolerated compared to the cationic Lipofectamine
686 RNAiMAX. PEG-DMG served a crucial role in maintaining lower particle diameters that likely
687 resulted in efficient uptake into primary rat cortical neurons. Our findings suggest that LNPs hold
688 promise for further silencing of therapeutically-relevant neuronal targets like TRPV1.
689
690 **Acknowledgements**
691
692 This work was supported via start-up funds for the Manickam laboratory from Duquesne
693 University (DU), a 2021 Faculty Development Fund (Office of Research, DU) and a 2021 Charles
694 Henry Leach II Fund to the PI (Duquesne University). We are grateful to Dr. Kathryn A.
695 Whitehead (Carnegie Mellon University) and her group for their support. We are grateful to Drs.
696 Jane E. Hartung and Michael S. Gold (University of Pittsburgh) for providing the DRG cultures.
697 We are also thankful to Dr. Wilson Meng and express our special appreciation to Mr. Nevil
698 Abraham (Duquesne University) for his help with the qPCR experiments. We express our
699 appreciation to Mr. Duncan Dobbins (Duquesne University) for his assistance with the graphical
700 abstract.
701

References

1. Wu SY, McMillan NAJ. Lipidic systems for in vivo siRNA delivery. AAPS J. 2009;11(4):639–52.
2. Wang J, Lu Z, Wientjes MG, Au JLS. Delivery of siRNA therapeutics: Barriers and carriers. AAPS J. 2010;12(4):492–503.
3. Akinc A, Maier M, Manoharan M, Fitzgerald K, Jayaraman M, Barros S, et al. The Onpattro story and the clinical translation of nanomedicines containing nucleic acid-based drugs. Nat Nanotechnol. 2019 Dec 1;14:1084–7.
4. FDA. FDA Approves First COVID-19 Vaccine. FDA News Release [Internet]. 2021; Available from: https://www.fda.gov/news-events/press-announcements/fda-approves-first-covid-19-vaccine
5. Ryan Cross. Without these lipid shells, there would be no mRNA vaccines for COVID-19. Chem Eng News. 2021;16–9.
6. Katakowski JA, Mukherjee G, Wilner SE, Maier KE, Harrison MT, Di Lorenzo TP, et al. Delivery of siRNAs to dendritic cells using DEC205-targeted lipid nanoparticles to inhibit immune responses. Mol Ther. 2016;24(1):146–55.
7. Uemura Y, Naoi T, Kanai Y, Kobayashi K. The efficiency of lipid nanoparticles with an original cationic lipid as a siRNA delivery system for macrophages and dendritic cells. Pharm Dev Technol. 2018 Apr 24;24:1–22.
8. Whitehead KA, Dorkin JR, Vegas AJ, Chang PH, Veiseh O, Matthews J, et al. Degradable lipid nanoparticles with predictable in vivo siRNA delivery activity. Nat Commun. 2014;5.
9. Lopes CDF, Gonçalves NP, Gomes CP, Saraiva MJ, Pêgo AP. BDNF gene delivery mediated by neuron-targeted nanoparticles is neuroprotective in peripheral nerve injury. Biomaterials. 2017;121:83–96.
10. Haney MJ, Klyachko NL, Zhao Y, Gupta R, Plotnikova EG, He Z, et al. Exosomes as drug delivery vehicles for Parkinson's disease therapy. J Control Release [Internet]. 2015;207:18–30. Available from: http://dx.doi.org/10.1016/j.jconrel.2015.03.033
11. Wolfe D, Mata M, Fink DJ. Targeted drug delivery to the peripheral nervous system using gene therapy. Neurosci Lett [Internet]. 2012;527(2):85–9. Available from: http://dx.doi.org/10.1016/j.neulet.2012.04.047
12. H. Ferreira-Vieira T, M. Guimaraes I, R. Silva F, M. Ribeiro F. Alzheimer's disease: Targeting the Cholinergic System. Curr Neuropharmacol. 2016;14(1):101–15.
13. Yang L, Han B, Zhang Z, Wang S, Bai Y, Zhang Y, et al. Extracellular vesicle-mediated delivery of circular RNA SCMH1 promotes functional recovery in rodent and nonhuman primate ischemic stroke models. Circulation. 2020;142(6):556–74.
14. Kim J, Jozic A, Sahay G. Naturally Derived Membrane Lipids Impact Nanoparticle-Based Messenger RNA Delivery. Cell Mol Bioeng. 2020;13(5):463–74.
15. Kulkarni JA, Witzigmann D, Chen S, Cullis PR, Van Der Meel R. Lipid Nanoparticle Technology for Clinical Translation of siRNA Therapeutics. Acc Chem Res. 2019;52(9):2435–44.
16. Rehman ZU, Zuhorn IS, Hoekstra D. How cationic lipids transfer nucleic acids into cells and across cellular membranes: Recent advances. J Control Release [Internet]. 2013;166(1):46–56. Available from: http://dx.doi.org/10.1016/j.jconrel.2012.12.014
17. Soenen SJH, Brisson AR, De Cuyper M. Addressing the problem of cationic lipid-

748 mediated toxicity: The magnetoliposome model. Biomaterials [Internet].
749 2009;30(22):3691–701. Available from:
750 http://dx.doi.org/10.1016/j.biomaterials.2009.03.040
751 18. Dahlman J, Kauffman K, Langer R, Anderson D. Nanotechnology for In vivo Targeted
752 siRNA Delivery. Adv Genet. 2014 Nov 21;88:37–69.
753 19. Wan C, Allen T, Cullis P. Lipid nanoparticle delivery systems for siRNA-based
754 therapeutics. Drug Deliv Transl Res. 2014 Feb 1;4.
755 20. Love KT, Mahon KP, Levins CG, Whitehead KA, Querbes W, Dorkin JR, et al. Lipid-like
756 materials for low-dose, in vivo gene silencing. Proc Natl Acad Sci U S A.
757 2010;107(5):1864–9.
758 21. Novobrantseva TI, Borodovsky A, Wong J, Klebanov B, Zafari M, Yucius K, et al.
759 Systemic RNAi-mediated gene silencing in nonhuman primate and rodent myeloid cells.
760 Mol Ther - Nucleic Acids. 2012;1(1):e4.
761 22. Blakney AK, McKay PF, Yus BI, Aldon Y, Shattock RJ. Inside out: optimization of lipid
762 nanoparticle formulations for exterior complexation and in vivo delivery of saRNA. Gene
763 Ther [Internet]. 2019;26(9):363–72. Available from: http://dx.doi.org/10.1038/s41434-
764 019-0095-2
765 23. Naseri N, Valizadeh H, Zakeri-Milani P. Solid lipid nanoparticles and nanostructured lipid
766 carriers: Structure preparation and application. Adv Pharm Bull [Internet]. 2015;5(3):305–
767 13. Available from: http://dx.doi.org/10.15171/apb.2015.043
768 24. Cullis PR, Hope MJ. Lipid Nanoparticle Systems for Enabling Gene Therapies. Mol Ther
769 [Internet]. 2017;25(7):1467–75. Available from:
770 http://dx.doi.org/10.1016/j.ymthe.2017.03.013
771 25. J. Jones L, T. Yue S, Cheung Ching-Ying, L. Singer V. RNA Quantitation by
772 Fluorescence-Based Solution Assay- RiboGreen Reagent Characterization.pdf. Anal
773 Biochem [Internet]. 1998;374(265):368–74. Available from: http://files/191/J. Jones et al.
774 - 1998 - RNA Quantitation by Fluorescence-Based Solution As.pdf
775 26. Hartung JE, Gold MS. GCaMP as an indirect measure of electrical activity in rat
776 trigeminal ganglion neurons. Cell Calcium [Internet]. 2020;89(April):102225. Available
777 from: https://doi.org/10.1016/j.ceca.2020.102225
778 27. Dave KM, Ali L, Manickam DS. Characterization of the SIM-A9 cell line as a model of
779 activated microglia in the context of neuropathic pain. PLoS One [Internet]. 2020;15(4):1–
780 28. Available from: http://dx.doi.org/10.1371/journal.pone.0231597
781 28. Dave KM, Han L, Jackson MA, Kadlecik L, Duvall CL, S Manickam D. DNA Polyplexes
782 of a Phosphorylcholine-Based Zwitterionic Polymer for Gene Delivery. Pharm Res.
783 2020;37(9).
784 29. Dave KM, Zhao W, Hoover C, D'Souza A, S Manickam D. Extracellular Vesicles
785 Derived from a Human Brain Endothelial Cell Line Increase Cellular ATP Levels. AAPS
786 PharmSciTech. 2021;22(1).
787 30. Honary S, Zahir F. Effect of zeta potential on the properties of nano-drug delivery systems
788 - A review (Part 1). Trop J Pharm Res. 2013;12(2):255–64.
789 31. Ing LY, Zin NM, Sarwar A, Katas H. Antifungal activity of chitosan nanoparticles and
790 correlation with their physical properties. Int J Biomater. 2012;2012.
791 32. Li X, Sloat BR, Yanasarn N, Cui Z. Relationship between the size of nanoparticles and
792 their adjuvant activity: Data from a study with an improved experimental design. Eur J
793 Pharm Biopharm. 2011;78(1):107–16.

794 33. Breznan D, Das DD, Mackinnon-Roy C, Bernatchez S, Sayari A, Hill M, et al.
795 Physicochemical Properties Can Be Key Determinants of Mesoporous Silica Nanoparticle
796 Potency in Vitro. ACS Nano. 2018;12(12):12062–79.
797 34. Shin SW, Song IH, Um SH. Role of physicochemical properties in nanoparticle toxicity.
798 Nanomaterials. 2015;5(3):1351–65.
799 35. Navya PN, Daima HK. Rational engineering of physicochemical properties of
800 nanomaterials for biomedical applications with nanotoxicological perspectives. Nano
801 Converg. 2016;3(1):1–14.
802 36. Braakhuis HM, Park MVDZ, Gosens I, De Jong WH, Cassee FR. Physicochemical
803 characteristics of nanomaterials that affect pulmonary inflammation. Part Fibre Toxicol.
804 2014;11(1).
805 37. Witzigmann D, Kulkarni JA, Leung J, Chen S, Cullis PR, Meel R Van Der. Since January
806 2020 Elsevier has created a COVID-19 resource centre with free information in English
807 and Mandarin on the novel coronavirus COVID- 19 . The COVID-19 resource centre is
808 hosted on Elsevier Connect , the company ' s public news and information .
809 2020;(January).
810 38. Chen S, Tam YYC, Lin PJC, Leung AKK, Tam YK, Cullis PR. Development of lipid
811 nanoparticle formulations of siRNA for hepatocyte gene silencing following subcutaneous
812 administration. J Control Release [Internet]. 2014;196:106–12. Available from:
813 http://dx.doi.org/10.1016/j.jconrel.2014.09.025
814 39. Romberg B, Hennink WE, Storm G. Sheddable coatings for long-circulating
815 nanoparticles. Pharm Res. 2008;25(1):55–71.
816 40. Kulkarni JA, Darjuan MM, Mercer JE, Chen S, Van Der Meel R, Thewalt JL, et al. On the
817 Formation and Morphology of Lipid Nanoparticles Containing Ionizable Cationic Lipids
818 and siRNA. ACS Nano. 2018;12(5):4787–95.
819 41. Malvern Panalytical. CORRELATION INTERCEPT – WHAT IS IT AND WHAT DOES
820 IT MEAN? [Internet]. Available from: https://www.materials-
821 talks.com/blog/2020/03/10/correlation-intercept-what-is-it-and-what-does-it-mean/
822 42. Pecze L, Jósvay K, Blum W, Petrovics G, Vizler C, Oláh Z, et al. Activation of
823 endogenous TRPV1 fails to induce overstimulation-based cytotoxicity in breast and
824 prostate cancer cells but not in pain-sensing neurons. Biochim Biophys Acta - Mol Cell
825 Res [Internet]. 2016;1863(8):2054–64. Available from:
826 http://dx.doi.org/10.1016/j.bbamcr.2016.05.007
827 43. Esposito MF, Malayil R, Hanes M, Deer T. Unique Characteristics of the Dorsal Root
828 Ganglion as a Target for Neuromodulation. Pain Med (United States). 2019;20:S23–30.
829 44. Yu X, Liu H, Hamel KA, Morvan MG, Yu S, Leff J, et al. Dorsal root ganglion
830 macrophages contribute to both the initiation and persistence of neuropathic pain. Nat
831 Commun [Internet]. 2020;11(1):1–12. Available from: http://dx.doi.org/10.1038/s41467-
832 019-13839-2
833 45. Xu Q, Zhang XM, Duan KZ, Gu XY, Han M, Liu BL, et al. Peripheral tgf-β1 signaling is
834 a critical event in bone cancer-induced hyperalgesia in rodents. J Neurosci.
835 2013;33(49):19099–111.
836 46. Moghimi SM, Symonds P, Murray JC, Hunter AC, Debska G, Szewczyk A. A two-stage
837 poly(ethylenimine)-mediated cytotoxicity: Implications for gene transfer/therapy. Mol
838 Ther. 2005;11(6):990–5.
839 47. Davey HM, Kell DB. Flow cytometry and cell sorting of heterogeneous microbial

840 populations: The importance of single-cell analyses. Microbiol Rev. 1996;60(4):641–96.
841 48. BIO-RAD. Flow Cytometry Data Analysis [Internet]. Available from: https://www.bio-
842 rad-antibodies.com/flow-cytometry-gating-
843 strategies.html?JSESSIONID_STERLING=1C53AF8B8470DB1019FE94619BC4BF4F.e
844 commerce1&evCntryLang=US-
845 en&cntry=US&thirdPartyCookieEnabled=true&wdLOR=cBC762A28-80AB-9C4A-
846 8B9C-0FF8F79509C6
847 49. Ryals RC, Patel S, Acosta C, McKinney M, Pennesi ME, Sahay G. The effects of
848 PEGylation on LNP based mRNA delivery to the eye. PLoS One [Internet]. 2020;15(10
849 October):1–17. Available from: http://dx.doi.org/10.1371/journal.pone.0241006
850 50. Chen S, Tam YYC, Lin PJC, Sung MMH, Tam YK, Cullis PR. Influence of particle size
851 on the in vivo potency of lipid nanoparticle formulations of siRNA. J Control Release
852 [Internet]. 2016;235:236–44. Available from:
853 http://dx.doi.org/10.1016/j.jconrel.2016.05.059
854 51. van der Meel R, Chen S, Zaifman J, Kulkarni J, Zhang XR, Tam Y, et al. Modular lipid
855 nanoparticle platform technology for siRNA and lipophilic prodrug delivery. bioRxiv.
856 2020;(2020).
857 52. Buyens K, Lucas B, Raemdonck K, Braeckmans K, Vercammen J, Hendrix J, et al. A fast
858 and sensitive method for measuring the integrity of siRNA-carrier complexes in full
859 human serum. J Control Release. 2008;126(1):67–76.
860 53. Walsh C, Ou K, Belliveau N, Leaver T, Wild A, Huft J, et al. Microfluidic-Based
861 Manufacture of siRNA-Lipid Nanoparticles for Therapeutic Applications. Methods Mol
862 Biol. 2014 Feb 25;1141:109–20.
863 54. Ball R, Bajaj P, Whitehead KA. Achieving long-term stability of lipid nanoparticles:
864 Examining the effect of pH, temperature, and lyophilization. Int J Nanomedicine.
865 2017;12:305–15.
866 55. Howard KA, Rahbek UL, Liu X, Damgaard CK, Glud SZ, Andersen M, et al. RNA
867 Interference in Vitro and in Vivo Using a Novel Chitosan/siRNA Nanoparticle System.
868 Mol Ther [Internet]. 2006;14(4):476–84. Available from:
869 http://dx.doi.org/10.1016/j.ymthe.2006.04.010
870 56. Thiramanas R, Li M, Jiang S, Landfester K, Mailänder V. Cellular Uptake of siRNA-
871 Loaded Nanocarriers to Knockdown PD-L1: Strategies to Improve T-cell Functions. Cells.
872 2020;9(9):1–12.
873 57. Mui1 BL, , Ying K Tam1 , Muthusamy Jayaraman2 , Steven M Ansell1 , Xinyao Du1 ,
874 Yuen Yi C Tam3 PJL, Chen3 S, Narayanannair2 JK, , Kallanthottathil G Rajeev2 ,
875 Muthiah Manoharan2 , Akin Akinc2 , Martin A Maier2 PC, Madden1 TD, et al. Influence
876 of Polyethylene Glycol Lipid Desorption Rates on Pharmacokinetics and
877 Pharmacodynamics of siRNA Lipid Nanoparticles. Mol Ther - Nucleic Acids.
878 2013;2(12):1–8.
879 58. Kulkarni JA, Cullis PR, Van Der Meel R. Lipid Nanoparticles Enabling Gene Therapies:
880 From Concepts to Clinical Utility. Nucleic Acid Ther. 2018;28(3):146–57.
881

Click here to access/download;Response to reviewers and editor;Response to Reviewers.pdf

Response to reviewers

We thank the reviewers for their insightful comments and helpful suggestions. We have addressed the comments and the individual responses to the questions are presented below. All new text (and figure titles) added in the revised manuscript in response to the reviewer's comments are highlighted in blue font.

Reviewer #1: The authors give a specific neural application of LNPs which is a hot topic during the COVID-19 pandemic. There are some points to clarify before publication:

1. Although a reference is cited in the section "Preparation of siRNA-loaded LNPs", this section can be described in more detail for the ease of understanding of readers out of the field. These parameters could be detailed: i) precise volume of ethanolic phase and aqueous phase used for the fabrication of LNPs should be cleared, ii) the 'slow mixing' and for the 'fast mixing' protocols should be explained in detail, iii) how the ethanol is removed from LNPs before application on the cells.

The precise volumes of the aqueous and ethanolic phases have been added to the revised manuscript in **Table 1**. We have also appended the protocols to include details of the 'slow' and 'fast' mixing in the methods section under '**Preparation of siRNA-loaded LNPs (siRNA-LNPs)'**. We treated cells with non-dialyzed LNPs and the concentration of ethanol in the transfection/treatment mixture was ca. 2% v/v. In our personal correspondence with Dr. Kathryn Whitehead (Carnegie Mellon University) ca. 2018, one of the pioneers in the development of siRNA-loaded LNPs, she indicated that non-dialyzed LNPs could be safely used on cells as long as the cells tolerated the formulations with no significant toxicity. We observed ~100% cell viabilities when cancer cell lines (MCF-7, MDA-MB-231 and BT-549) and primary DRG neurons were exposed to LNPs (**Figure 6**) and conclude that the non-dialyzed LNPs are safely tolerated by the cell models used in this study.

2. The colloidal stability of nanoparticles should be also checked at 37 C for 24 h since the cells were exposed to nanoparticles for 24 hours in 37 C. Testing the stability at 37 C reveals if the nanoparticles remain stable during this experiment. Additionally, it would be nice to have the results of the serum stability test results of LNPs to see if the developed LNPs are stable in this medium.

The colloidal stability of LNPs at 37°C for 24 h and in the presence of serum was studied and the results are presented in the revised manuscript as **Figures 3** and **4**. Our data showed that the LNP diameters and zeta potentials did no change appreciably 24 h post-preparation at 37 °C and LNP particle diameters were additionally stabilized in the presence of 10% FBS—suggesting that both these conditions did not affect their colloidal stability.

3. TEM imaging before and after incubation at 37 C for 24 h could be presented to prove the stability of LNPs.

As discussed above, we have used DLS measurements as a quantitative tool to demonstrate the stability of LNPs. We thank the reviewer for this important suggestion and are now establishing collaborative arrangements with the University of Pittsburgh to carry out cryo-TEM studies of LNPs and the results of these studies will be reported in a forthcoming manuscript.

4. In figure4, some of the graphs and the letters on these graphs are presented with the same color which makes it harder to follow and understand. This figure could be rebuilt with more clear structuring and coloring. Specifically, the graph lines with green color seem pixelized.

This figure has been re-worked to improve clarity in the revised manuscript (**Figure 7**). We would like to highlight a few things to explain the pixelization of the histogram. The green-colored histogram in **Figure 7** shows the percentage of positive cells for Cy5 (Cy5 (+)) when the neurons were treated with Cy5 siRNA/Lipofectamine RNAiMAX complexes. As expected, Lipofectamine RNAiMAX showed the highest (94.9 %) percentage of Cy5 (+) cells. As a result, neurons treated with Lipofectamine RNAiMAX showed the greatest shift towards the right. Interestingly, we also observed two distinct peaks (a "bimodal" histogram) for this group with varying Cy5 intensities as compared to a "unimodal" histogram for neurons treated with LNPs (**Figure 7c (yellow and brown)**). As RNAiMAX is toxic to cells, it is likely that the first peak corresponds to Cy5 siRNA taken up by distressed cells (resulting in lower Cy5 intensities). The second peak showed a greater percentage Cy5 (+) cells demonstrating the increased uptake of Cy5 siRNA by the viable cells. <u>The histogram corresponding the Lipofectamine groups appears to be pixelized as the histogram width is also broader for this treatment group compared to the LNP-treated neurons</u>. Moreover, the histograms depicted in **Figure 7** are autogenerated by the Attune NxT software of the Attune NxT Flow Cytometer. It should be pointed out that histograms reported in literature as well as those in the training and user guides of the Attune NxT Cytometer show a similar pattern of pixelization (1–4).

5. The fluorescent microscopy images presented in Figure5 seem blurry, they could be enhanced. Additionally, in Figure5b the cell morphology seems different than other cells specifically in the image of cells exposed to RNAİMAX complex (Cells treated with this complex are presented as viable after 4 h, it would be necessary to detail this finding).

The 'blurriness' of the fluorescent microscopy image presented in **Figure 8** (in the revised manuscript) is likely a result of the 'zoomed-out' micrographs presented in the figures. We have revised **Figure 8** by including a 'zoomed-in' version of one the LNP groups (cells treated with 50 nM Cy5 siRNA-LNPs+PEG-DMG in **panel d**. This image depicts a clearer view of the cells wherein the Cy5 siRNA LNPs show diffuse fluorescence in the cytoplasm. The reviewer has rightly pointed out the difference in morphology of cells exposed to Lipofectamine RNAiMAX in **panels b and c** in **Figure 8**. Lipofectamine RNAiMAX is a highly cationic lipid and a benchmark transfection agent for RNA molecules. Although a strong cationic charge serves to enhance the uptake of carrier molecules in cells, it concurrently mediates cell stress (5). <u>The observed changes in morphology of cells is a result of this Lipofectamine-mediated stress in this particular cell model, human cortical neurons</u>.

Reviewer #2: The author herein demonstrate performance of LNPs for siRNA delivery to neural cell. The study is interesting and deemed fit for publication in this journal. However, there are several limitations that must be addressed and discussed.

1. The author must perform a reporter assay. Only uptake does not guarantee successful siRNA delivery.

The reviewer makes an important comment here and we have indeed performed pilot experiments to study the knockdown of a therapeutic/neuron-relevant knockdown target. We had chosen not to include this data in the original submission due to the reasons discussed in the supplementary information, but this data is now included in the revised manuscript (**Supplementary Figure 3**). Primary dorsal root ganglion (DRG) neurons isolated from rat trigeminal ganglia were used to study the knockdown of transient receptor potential cation channel subfamily V member 1 (TRPV1), a neuron-relevant knockdown target. SiRNA against TRPV1 (siTRPV1) was chosen as a proof-of-concept drug because it has been reported that TPRV1 becomes hyperactive in response to chronic inflammatory pain that reduces their threshold for activation and increases sodium, calcium and chloride fluxes (7, 8). TRPV1 is a non-selective cation channel exhibiting high calcium permeability and is expressed in peripheral, central axon terminals in the spinal cord, C fibers and/or Aδ fibers (8). Nearly 60% of the peptidergic primary nociceptors in the dorsal root ganglia and trigeminal ganglia express TRPV1 (8). Primary DRG cultures were isolated using previously reported methods (9). The inherent technical challenges associated with isolating DRG neurons/cultures resulted in low numbers of isolated cells but we still proceeded with the transfection study to determine if this TRPV1 target can be silenced using siTRPV1 delivered via LNPs (10–12).

A key limitation of this study is that the low numbers of neurons (2,500 cells/well) used will naturally have a low (or rather a very low) baseline expression of TRPV1 and therefore, this current setting does not allow us to optimally determine the effectiveness of siTRPV1 delivery via LNPs. Proceeding with this caveat, we cautiously discuss here the findings from this experiment. siTRPV1-LNPs (+PEG-DMG) were formulated using C12-200, an ionizable cationic lipid and helper lipids. The resulting mRNA levels post-transfection were determined using quantitative reverse transcription PCR. Our data showed a low 9% knockdown of TRPV1 when primary DRG cultures were treated with siTRPV1-LNPs that was similar to cells treated with the positive control, siTRPV1-Lipofectamine RNAiMAX complexes. Cells treated with naked siTRPV1-LNPs showed around 2.6% knockdown of TRPV1 whereas inverted (inv.) siTRPV1-LNPs showed about 3.2% TRPV1 knockdown. Despite the low levels of knockdown, the observed differences in % knockdown were significant (****$p < 0.0001$). As stated earlier in this section, this pilot study must be carefully interpreted due to the caveats associated with the low cell numbers and therefore, a lower baseline TRPV1 expression. Nevertheless, this data points out the safety and the potential of LNPs as delivery agents to silence therapeutically-relevant neuronal targets. Current efforts are underway in the laboratory to establish primary neuronal cultures with a higher yield and results of those studies will be reported in a forthcoming manuscript.

2. The authors just selected one concentration to show cytocompatibility. The cytocompatibility of the LNPs and control lipids must be performed in a dose escalation setting for better comparison.

The cytocompatibility data of LNPs tested at increasing doses of siGFP LNPs is now included in the revised manuscript (**Figure 6c**).

3. The intensity and autocorrelation function of DLS measurement must be included. This reviewer strongly recommends comparing autocorrelation function at different time point to get insights into their stability.

The intensity and autocorrelation function of DLS measurement is now included in the revised manuscript in **Figure 4**. We have also compared the autocorrelation function at different time points and is now included in the revised manuscript as **Table 2**.

4. The author must stain the live cells. Besides, the microscopy pictures are of poor resolution.

The 'blurriness' of the fluorescent microscopy image presented in **Figure 8** (in the revised manuscript) is likely a result of the 'zoomed-out' micrographs presented in the figures. We have revised **Figure 8** by including a 'zoomed-in' version of one the LNP groups (cells treated with 50 nM Cy5 siRNA-LNPs+PEG-DMG) in **panel d**. This image depicts a clearer view of the cells wherein the LNP-delivered siRNA shows diffuse fluorescence in the cytoplasm.

5. The LNP preparation methods need clarification. How much volume of 1 mg/mL siRNA solution was prepared? The author must mention the cat# for each siRNA used.

The precise volumes of the aqueous and ethanolic phases have been added to the revised manuscript in **Table 1**. We have also appended the protocols for 'slow' and 'fast' mixing in the methods section under '**Preparation of siRNA-loaded LNPs (siRNA-LNPs)'**. The catalog numbers of the siRNAs are now included in the **'Materials'** section of the revised manuscript.

6. In LNP preparation, why the author chose to dilute instead of dialysis/similar technique to replace the citrate buffer with PBS? What's the final pH of the solution? This is important to report the zetapotential, as it is highly pH dependent. Depending on volume of citrate and PBS used for LNP preparation for different experiment their charge and size may get affected.

In our personal correspondence with Dr. Kathryn Whitehead (Carnegie Mellon University) ca. 2018, one of the pioneers in the development of siRNA-loaded LNPs, she indicated that non-dialyzed LNPs could be safely used on cells as long as the cells tolerated the formulations with no significant toxicity. We observed ~100% cell viabilities when cancer cell lines (MCF-7, MDA-

MB-231 and BT-549) and primary DRG neurons were exposed to LNPs (**Figure 6**) and conclude that the non-dialyzed LNPs are safely tolerated by the cell models used in this study.

The final pH of the solution is 7.4 (now included in the legend for **Figure 2** in the revised manuscript).

7. The method section must include statistical analysis. Two-way ANOVA and not one-way should be performed whenever applicable.

We have now added statistical analysis in the **'Methods'** section of the revised manuscript. We used either one-way ANOVA or two-way ANOVA along with One-Sample T- and Wilcoxon tests based on the recommendations from GraphPad Prism software.

References

1. ThermoFisher. Imaging-enhanced flow cytometry [Internet]. Available from: https://www.thermofisher.com/us/en/home/life-science/cell-analysis/flow-cytometry/flow-cytometers/attune-nxt-flow-cytometer/sample-data.html
2. Life Technologies. Attune ® acoustic focusing cytometer training guide. 2010;(MAN0002736):2–6.
3. ThermoFisher Scientific. Attune ™ NxT Software User Guide. 2019;(100024236).
4. Flegel K, Sun D, Grushko O, Ma Y, Buttitta L. Live cell cycle analysis of Drosophila tissues using the attune acoustic focusing cytometer and vybrant dyecycle violet DNA stain. J Vis Exp. 2013;(75):1–7.
5. Soenen SJH, Brisson AR, De Cuyper M. Addressing the problem of cationic lipid-mediated toxicity: The magnetoliposome model. Biomaterials [Internet]. 2009;30(22):3691–701. Available from: http://dx.doi.org/10.1016/j.biomaterials.2009.03.040
6. Huang J, Zhang X, McNaughton P. Inflammatory Pain: The Cellular Basis of Heat Hyperalgesia. Curr Neuropharmacol. 2006;4(3):197–206.
7. Tominaga M, Wada M, Masu M. Potentiation of capsaicin receptor activity by metabotropic ATP receptors as a possible mechanism for ATP-evoked pain and hyperalgesia. Proc Natl Acad Sci U S A. 2001;98(12):6951–6.
8. Finnerup NB, Attal N, Haroutounian S, McNicol E, Baron R, Dworkin RH, et al. Pharmacotherapy for neuropathic pain in adults: Systematic review, meta-analysis and updated NeuPSig recommendations. Lancet Neurol. 2015;14(2):162–73.
9. Hartung JE, Gold MS. GCaMP as an indirect measure of electrical activity in rat trigeminal ganglion neurons. Cell Calcium [Internet]. 2020;89(April):102225. Available from: https://doi.org/10.1016/j.ceca.2020.102225
10. Shen H, Gan M, Yang H, Zou J. An integrated cell isolation and purification method for rat dorsal root ganglion neurons. J Int Med Res [Internet]. 2019;47(7):3253–60. Available from: https://doi.org/10.1177/0300060519855585

11. Jennifer Gordon, Shohreh Amini and MKW. General overview of neuronal cell culture. Methods Mol Biol [Internet]. 2013;1078:35–44. Available from: http://link.springer.com/10.1007/978-1-62703-640-5

12. Klimovich P, Rubina K, Sysoeva V, Semina E. Three-dimensional model of dorsal root ganglion explant as a method of studying neurotrophic factors in regenerative medicine. Biomedicines. 2020;8(3).

Click here to access/download;Graphical Abstract;Revision_Graphical Abstract.tif

Lipidoid nanoparticles increase siRNA uptake into primary neurons

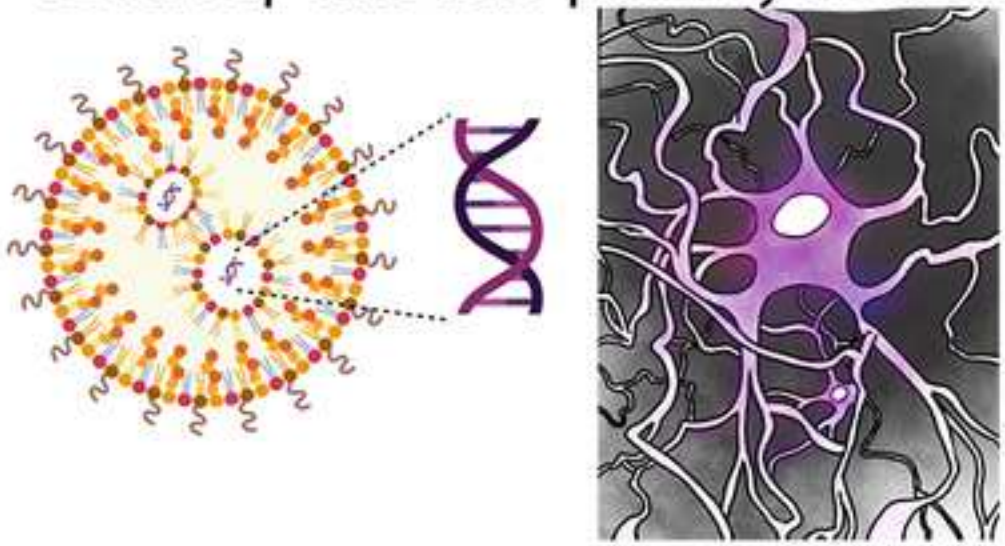

Figure 1

Click here to access/download;Figure;Figure 1.tif

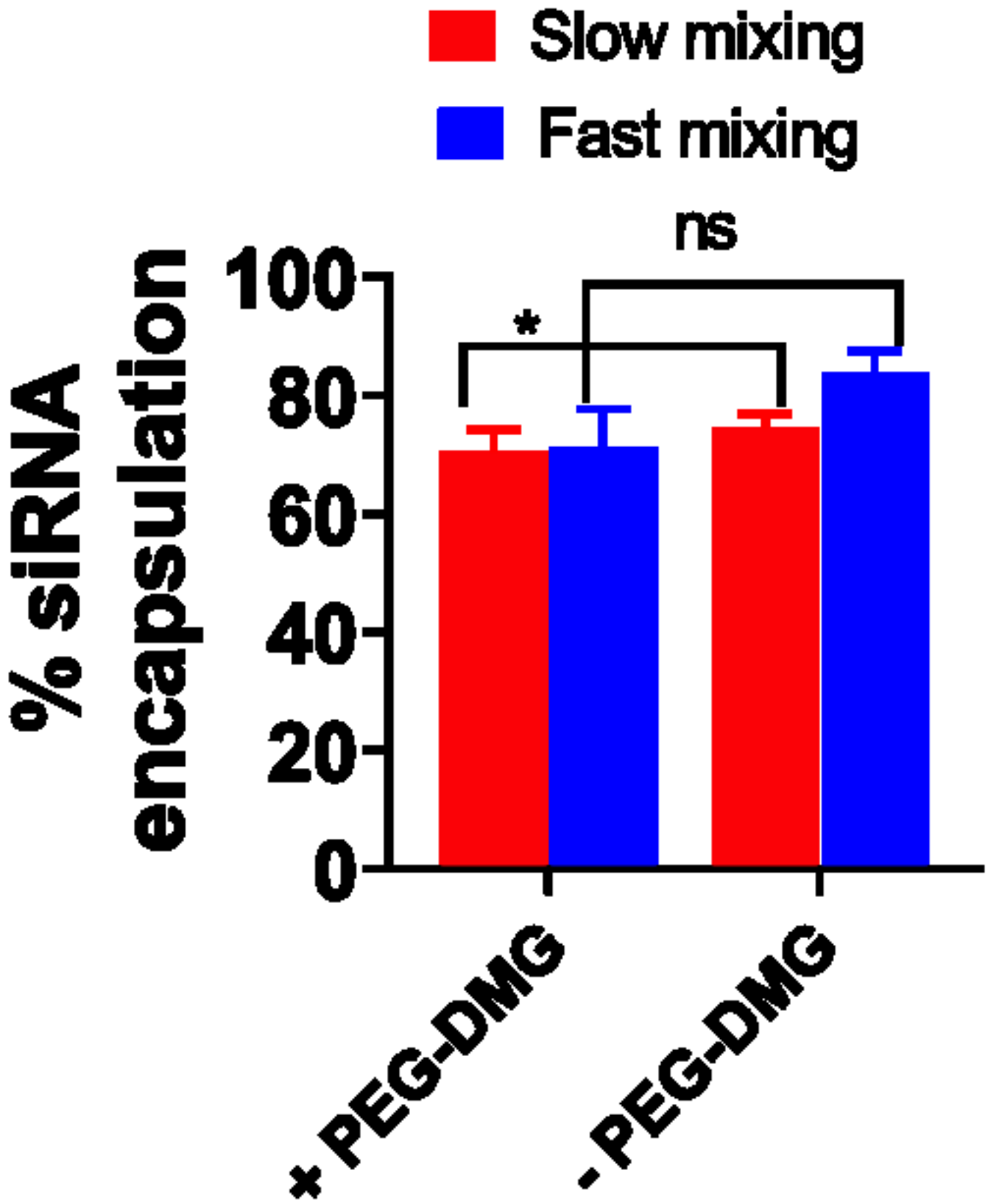

Figure 2

Click here to access/download;Figure;Figure 2.tiff

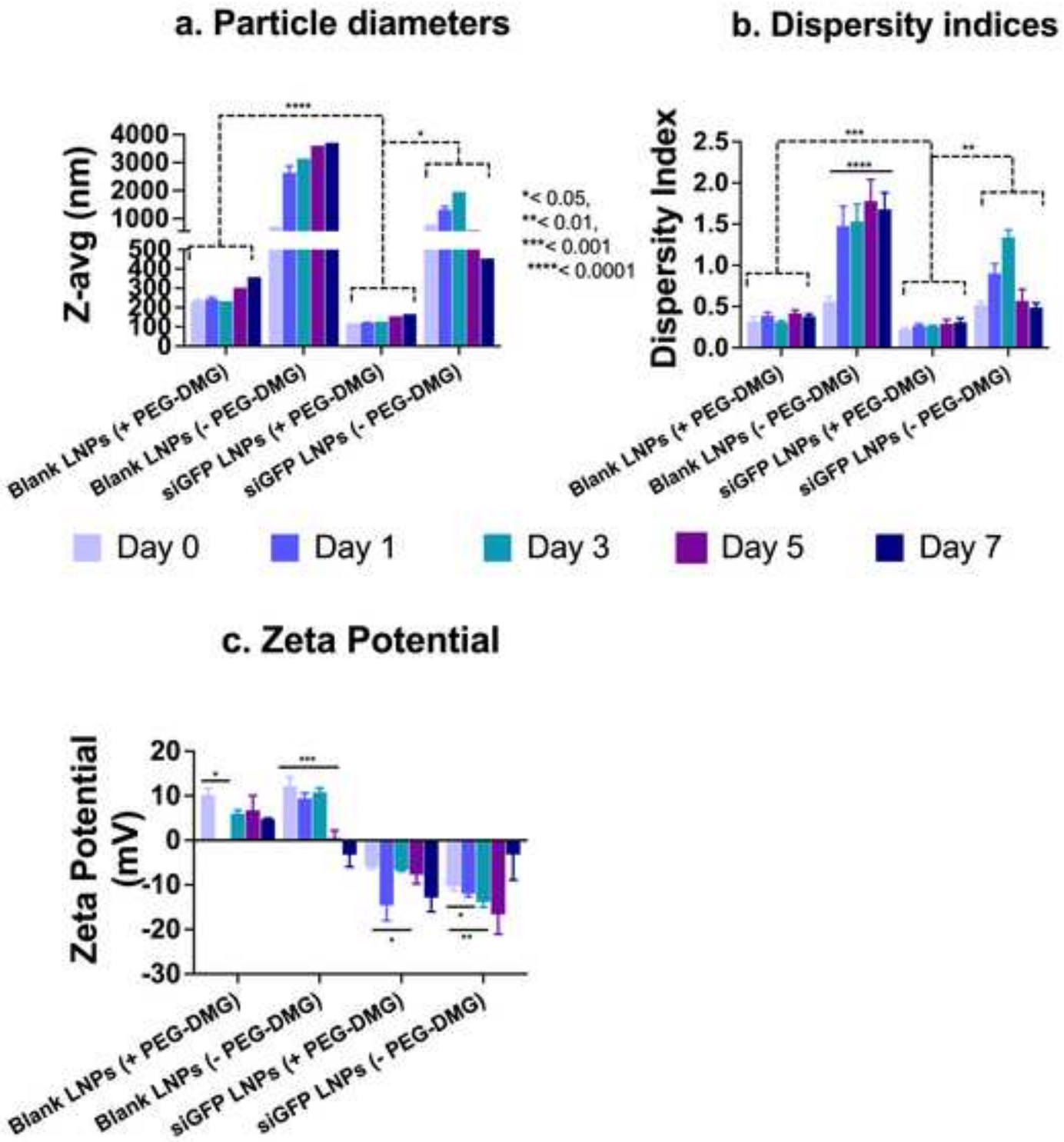

Figure 3

Click here to access/download;Figure;Figure 3.tiff

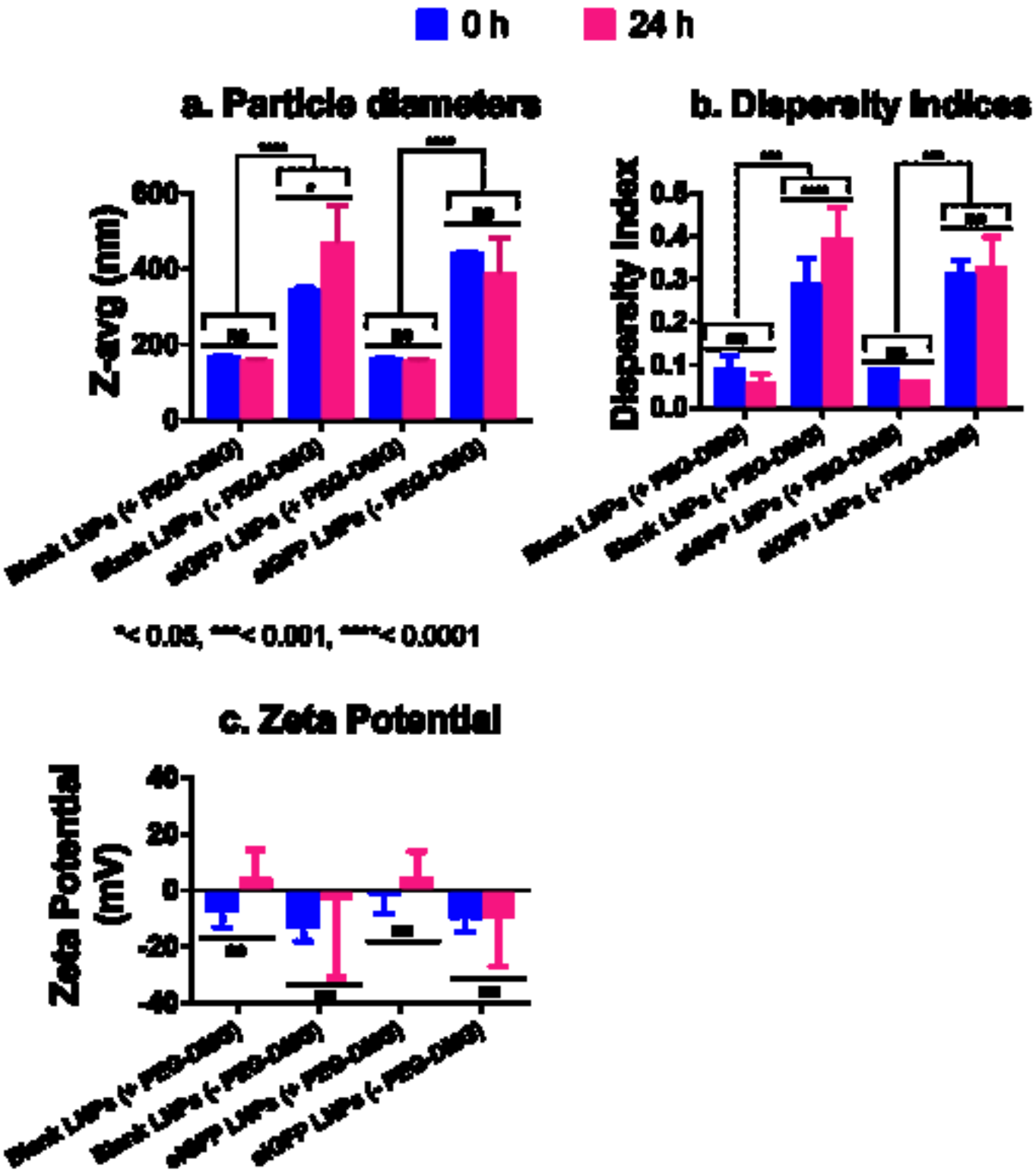

Figure 4

Click here to access/download;Figure;Figure 4.tiff

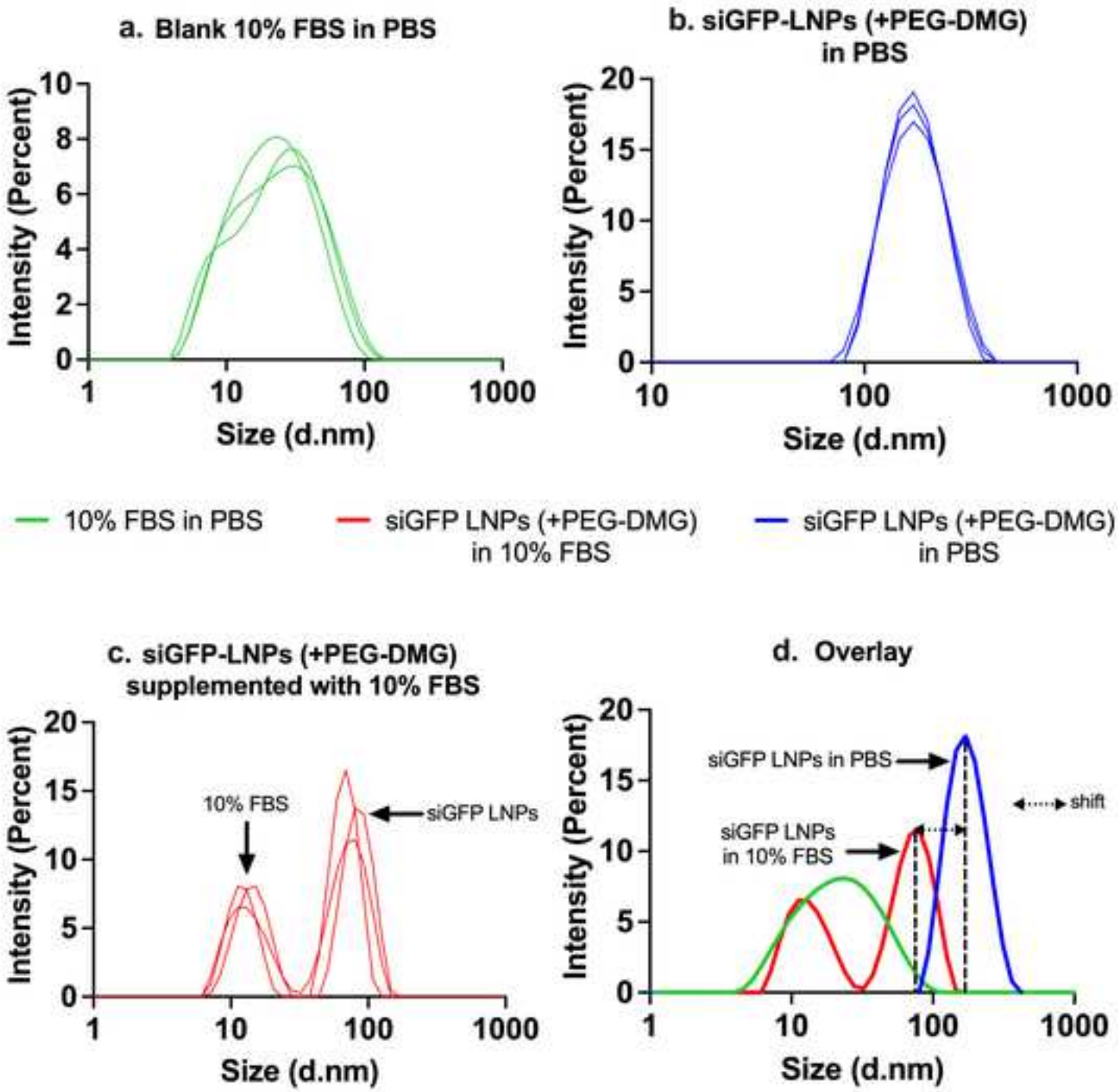

Figure 5

Click here to access/download;Figure;Figure 5.tiff

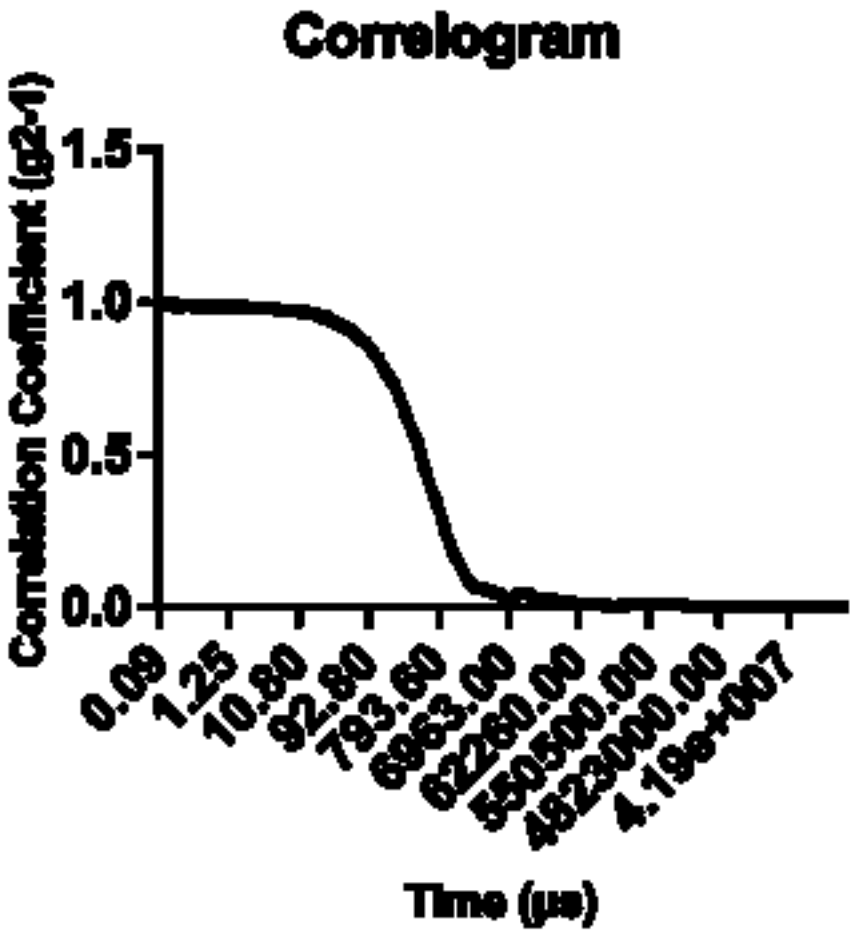

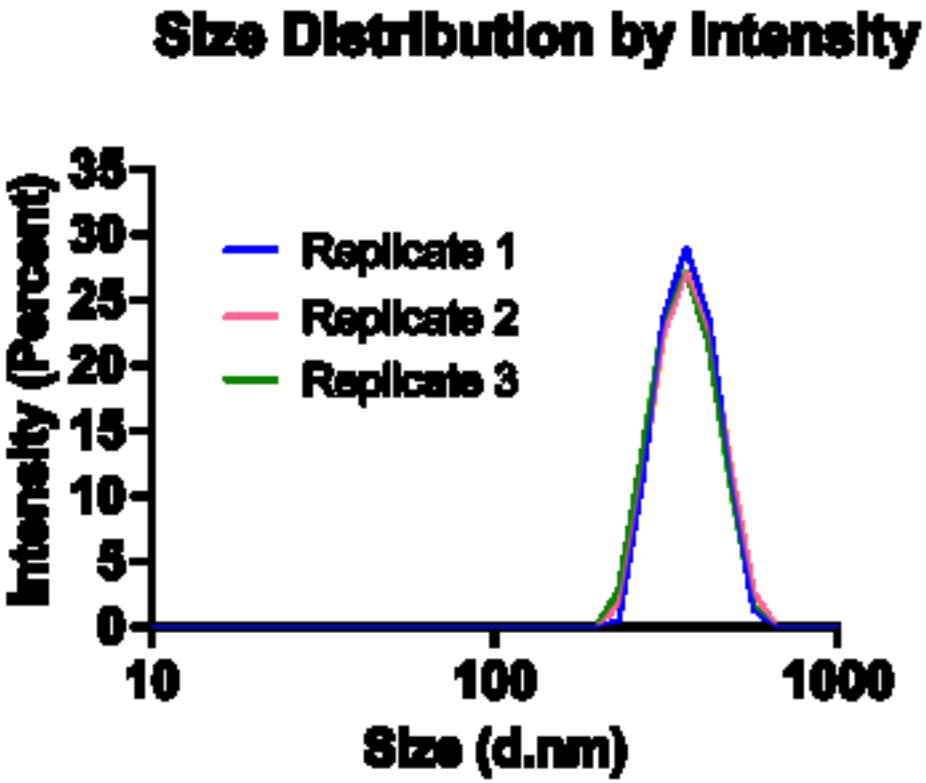

Figure 6

Click here to access/download;Figure;Figure 6.tiff

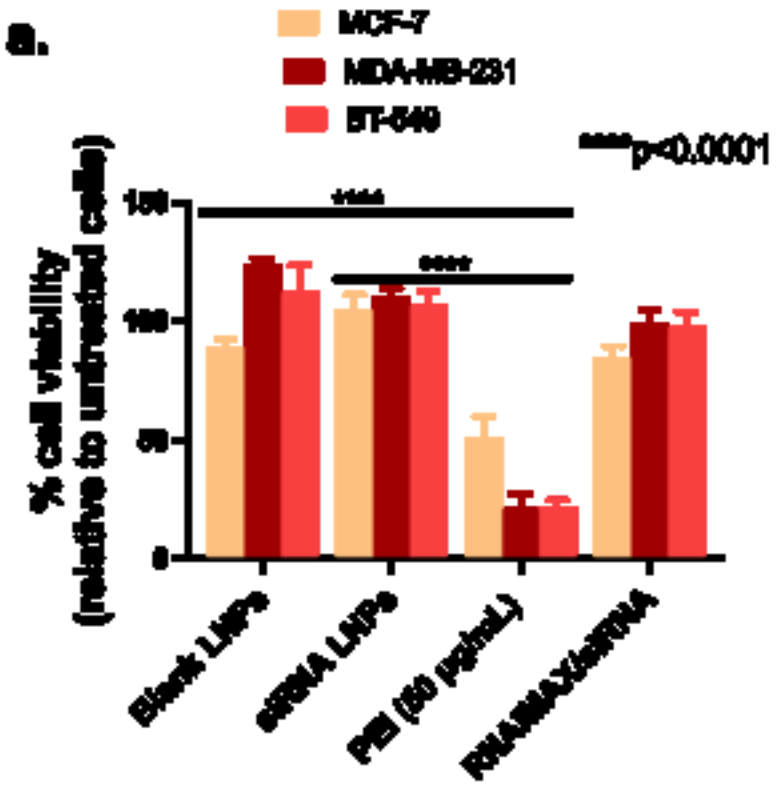

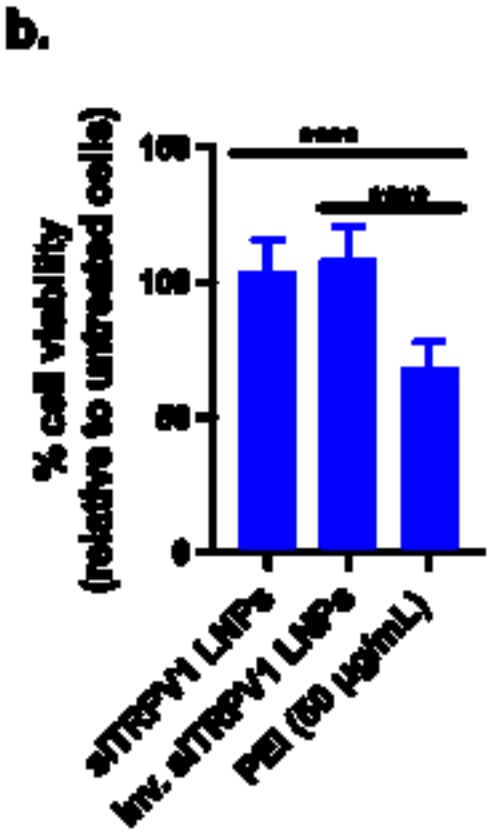

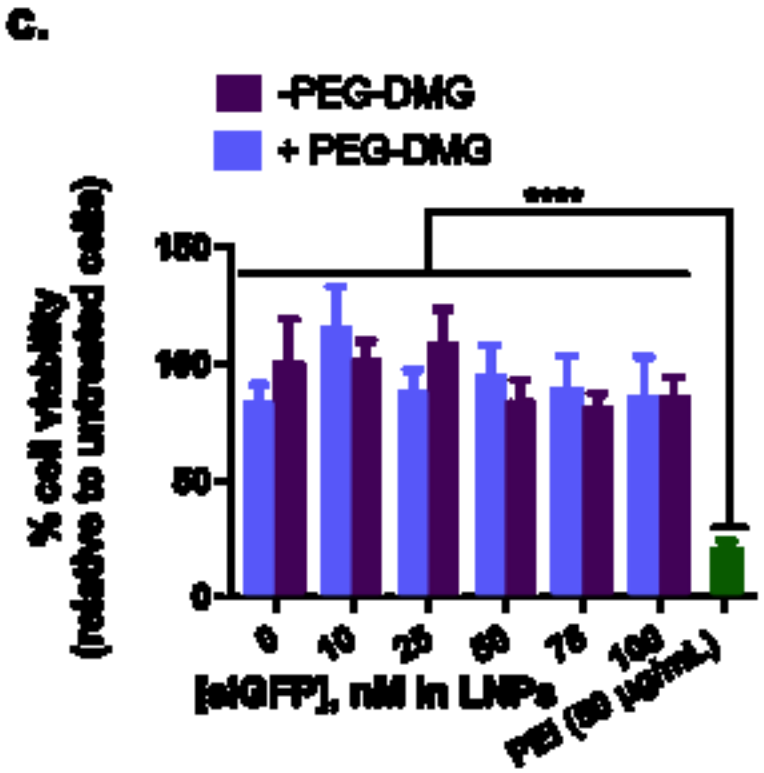

Figure 7

Click here to access/download;Figure;Figure 7.tiff

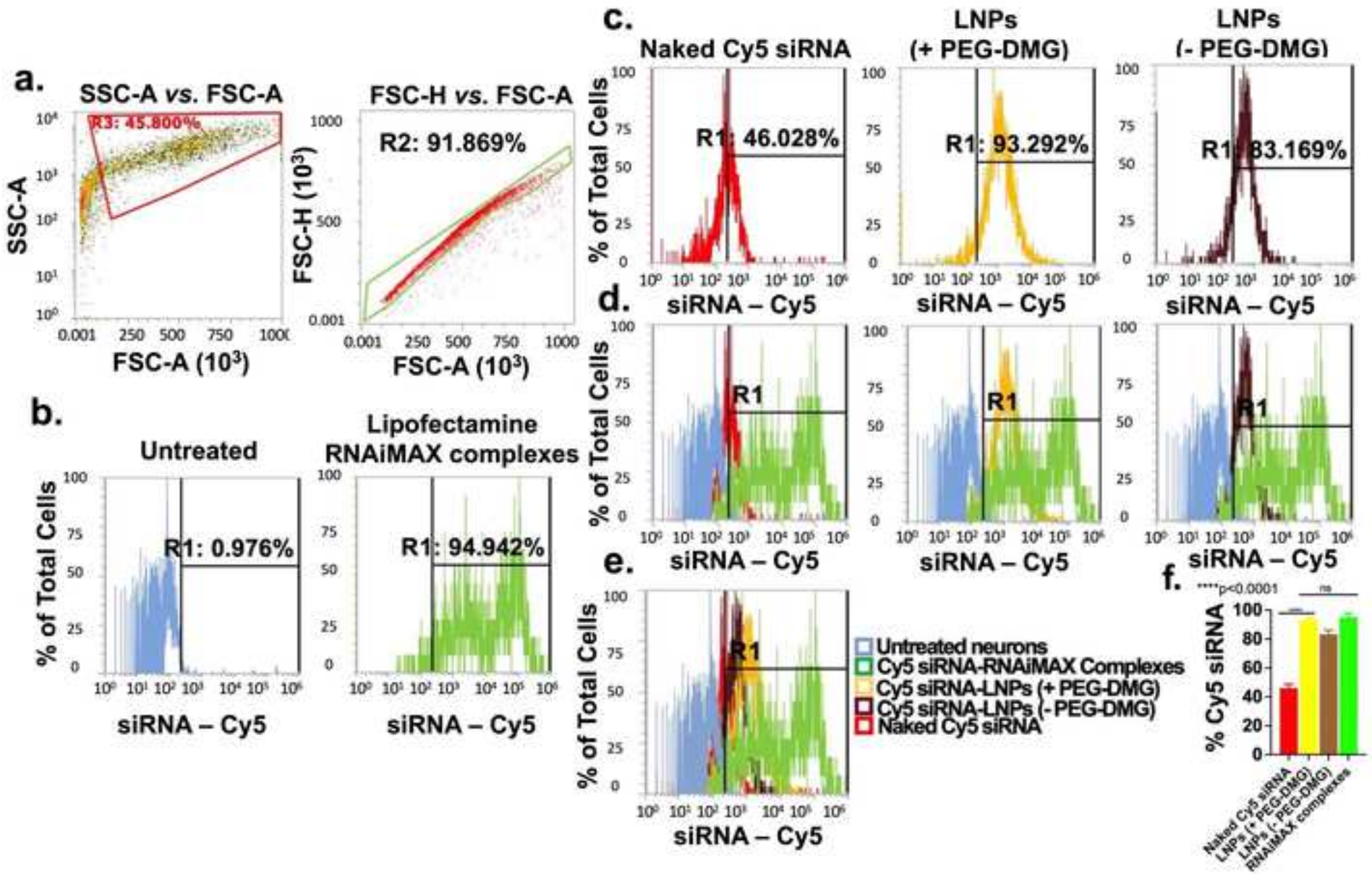

Figure 8

Click here to access/download;Figure;Figure 8.tiff

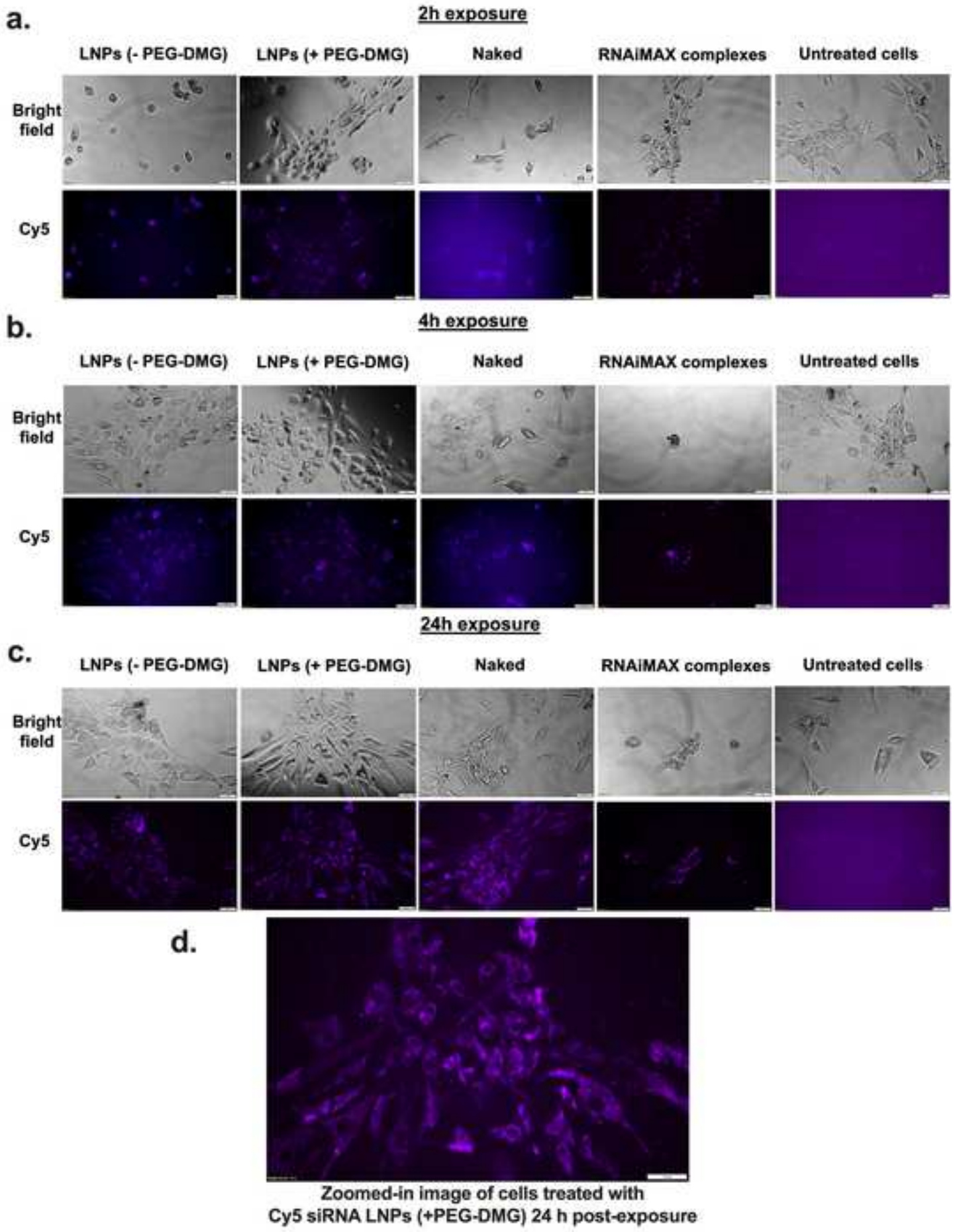

Zoomed-in image of cells treated with Cy5 siRNA LNPs (+PEG-DMG) 24 h post-exposure

Supplementary Figure 1

Click here to access/download;Figure;Figure S1.tif

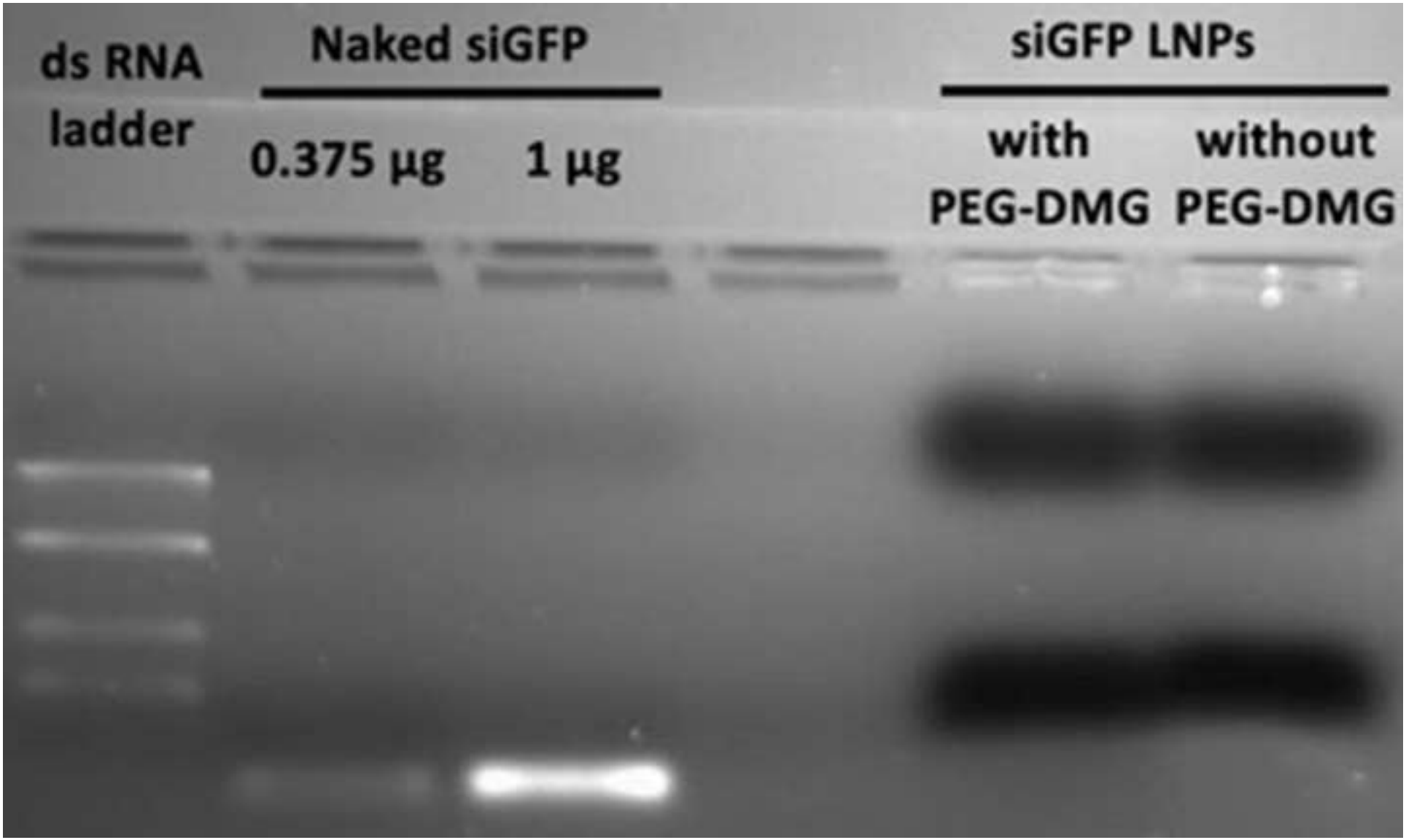

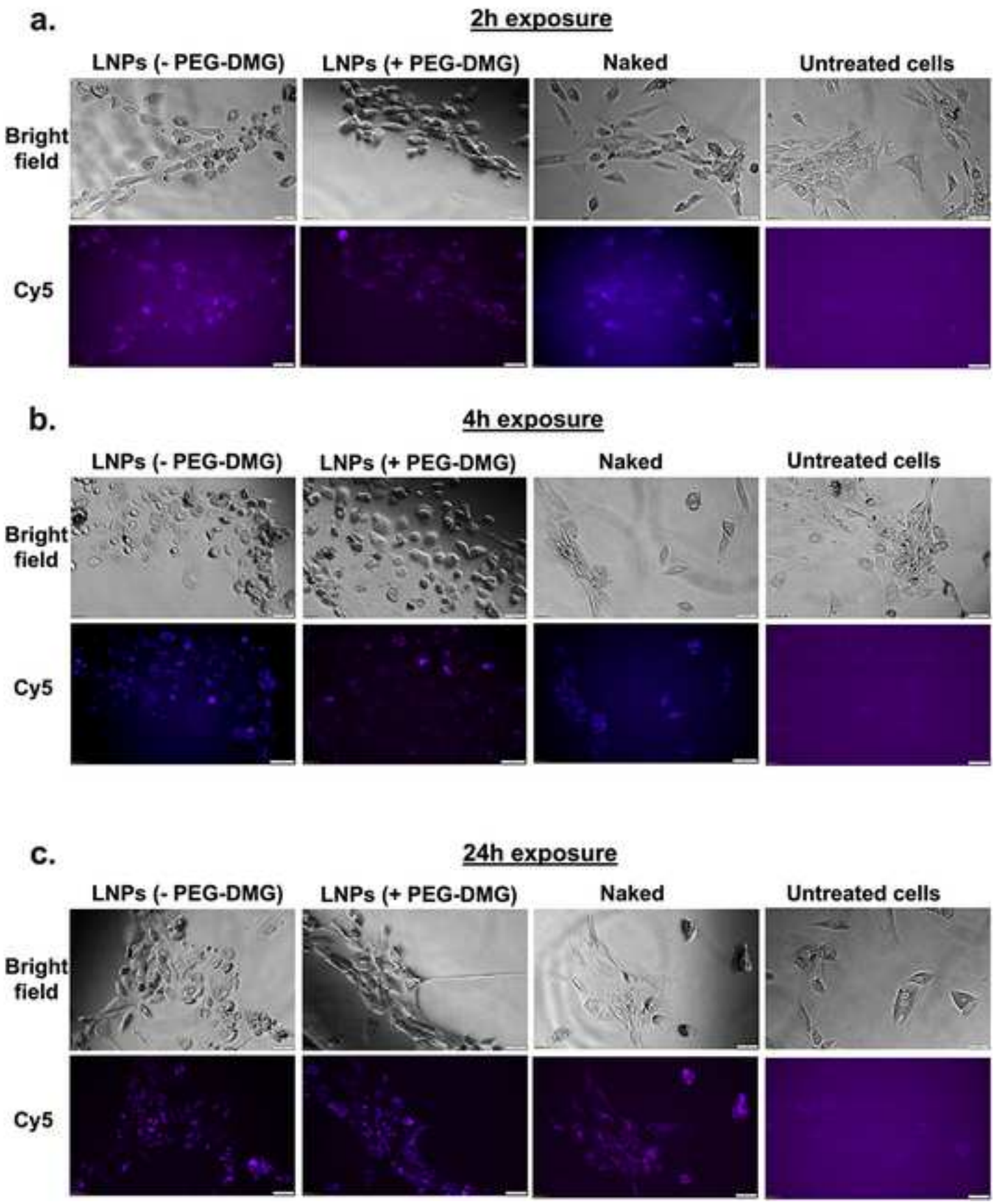
a.
2h exposure
LNPs (- PEG-DMG)
LNPs (+ PEG-DMG)
Naked
Untreated cells
Bright field
Cy5
b.
4h exposure
LNPs (- PEG-DMG)
LNPs (+ PEG-DMG)
Naked
Untreated cells
Bright field
Cy5
c.
24h exposure
LNPs (- PEG-DMG)
LNPs (+ PEG-DMG)
Naked
Untreated cells
Bright field
Cy5

Supplementary Figure 3

Click here to access/download;Figure;Figure S3.tiff

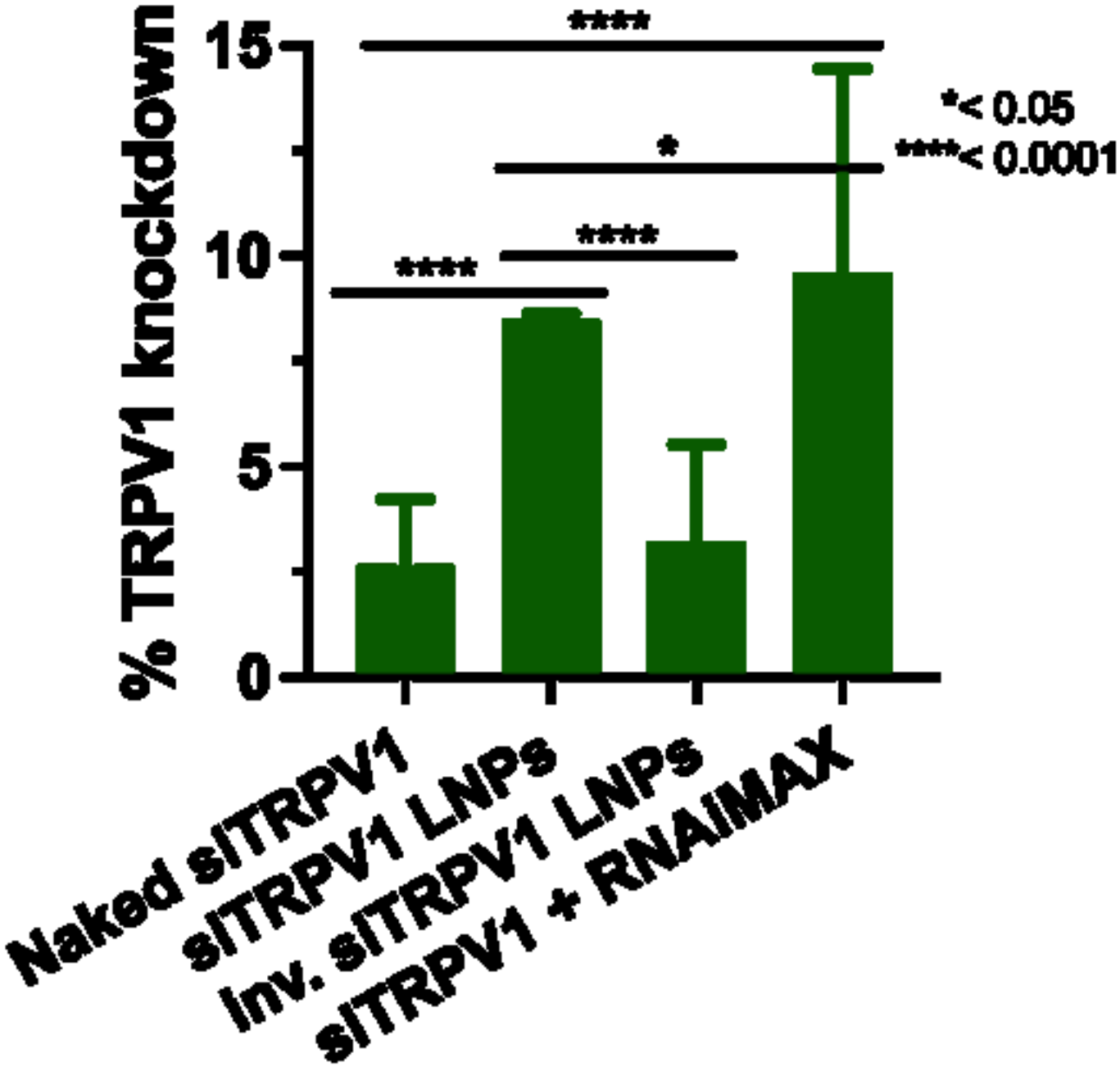

Click here to access/download
Author Supplementary Files (excel worksheets, video in mpeg-1 format only , etc)
Revision_Supplementary Information.pdf